nature nanotechnology

REVIEW ARTICLE

PUBLISHED ONLINE: 6 JUNE 2017 | DOI: 10.1038/NNANO.2017.72

Fundamental transport mechanisms, fabrication and potential applications of nanoporous atomically thin membranes

Luda Wang, Michael S. H. Boutilier, Piran R. Kidambi, Doojoon Jang, Nicolas G. Hadjiconstantinou and Rohit Karnik*

Graphene and other two-dimensional materials offer a new approach to controlling mass transport at the nanoscale. These materials can sustain nanoscale pores in their rigid lattices and due to their minimum possible material thickness, high mechanical strength and chemical robustness, they could be used to address persistent challenges in membrane separations. Here we discuss theoretical and experimental developments in the emerging field of nanoporous atomically thin membranes, focusing on the fundamental mechanisms of gas- and liquid-phase transport, membrane fabrication techniques and advances towards practical application. We highlight potential functional characteristics of the membranes and discuss applications where they are expected to offer advantages. Finally, we outline the major scientific questions and technological challenges that need to be addressed to bridge the gap from theoretical simulations and proof-of-concept experiments to real-world applications.

Membranes are thin barriers that permit selective mass transport, and form the basis of a number of separation processes typically driven by gradients in pressure, electric potential, concentration or temperature[1,2]. With the advantages of modularity, scalability, compactness and high energy efficiency, membrane separations have become pervasive[3] in applications related to energy[4], water[5], food[6], biotechnology[7] and chemical processing[3]. Major applications include water desalination[8–10], natural gas purification[11], production of nitrogen from air[1], haemodialysis[12], bioprocessing[7], solvent- and petrochemical-based separations[13,14], and production of ultrapure water[15]. Beyond separations, membranes find use in fuel cells[4], drug delivery[12], bio/chemical sensors[16] and energy harvesting from mixing processes[5].

The performance of membrane-based systems (for example, energy efficiency, productivity or product recovery) depends on the constituent membrane characteristics, which place constraints on and define trade-offs in membrane process design. In addition to being economical and manufacturable, an ideal membrane should easily allow flow of the desired species (high permeance), reject undesired species (high selectivity) and exhibit robustness in operation (high chemical, mechanical and thermal stability, low fouling) (see Box 1).

Although remarkable progress has been achieved in membrane technology, persistent challenges remain, specifically (1) overcoming the trade-off between selectivity and permeability of the membrane material, (2) mitigation of fouling and (3) robust operation under harsh conditions. Specific examples include the need for chlorine-resistant membranes for water desalination[5,10,17] and high-permeance membranes for production of oxygen from air[1]. To address these challenges, the past few decades have seen the exploration of various membrane structures and materials, including novel polymers[1], inorganic membranes (zeolites[18], silica, carbon[19], ceramics), nanomaterials (metal-organic frameworks[20], carbon nanotubes[21] (CNTs), carbon nanomembranes[22]) and polymer–inorganic 'mixed-matrix' membranes[1,19], among others. These developments seek to achieve improved membrane performance by (1) the use of favourable membrane structures, for example, a thin selective layer, or (2) the use of materials with favourable properties, for example, antifouling properties and frictionless transport in CNTs[23], or high permeability and selectivity of materials with intrinsic porosity[24].

The rise of graphene and other atomically thin materials in the past decade[25] has opened new possibilities in membrane technology. The atomic thickness of these materials makes them the thinnest possible barrier[26], which, combined with their remarkable mechanical strength[27], chemical robustness[28] and ability to sustain selective, nanometre-scale pores[29], evokes the possibility — at least in principle — of realizing an ideal nanoporous atomically thin membrane that could be tailored to a range of applications while offering high permeance, high selectivity and high chemical resistance. This review focuses on nanoporous atomically thin membranes (NATMs)[30–37] where transport is governed by flow across rigid pores in a continuous, atomically thin layer; for a discussion of membranes where other mechanisms influence transport, such as graphene oxide or carbon nanomembranes, the reader is directed to several excellent reviews[22,32,38–41].

Transport mechanisms

Membranes achieve selective transport through a variety of mechanisms operative over different length scales (Fig. 1a). At the smallest scale, dense polymeric membranes (without defined pores), such as reverse osmosis membranes for water desalination and many gas separation membranes, operate by a solution-diffusion mechanism[1,42]. Here, selectivity results from differences in species solubilities and diffusivities in the membrane material; solubility depends on the molecular structure, membrane porosity and chemical affinity, whereas diffusivity is governed by thermally activated rearrangements of the polymer chains that strongly favour size-dependent diffusion of smaller molecules. When selectivity

Department of Mechanical Engineering, Massachusetts Institute of Technology, 77 Massachusetts Avenue, Cambridge, Massachusetts 02139, USA.
*e-mail: karnik@mit.edu

Box 1 | Definitions, transport equations and length scales for NATMs.

Definitions of transport properties

$$\text{Permeance} \equiv \frac{\text{Mass, volume or molar flow rate across membrane}}{\text{Membrane area} \times \text{Pressure difference}}$$

where 'pressure difference' may also refer to a difference in chemical potential, concentration, electric potential and so on.

$$\text{Selectivity} \equiv \frac{\text{Permeance of species A}}{\text{Permeance of species B}}$$

$$\text{Rejection} \equiv 1 - \frac{\text{Solute concentration in permeate solution}}{\text{Solute concentration in feed solution}}$$

$$\text{Pore permeation coefficient} \equiv \frac{\text{Mass, volume or molar flow rate across pore}}{\text{Pressure difference}}$$

$$\text{Pore effective area} \equiv \frac{\text{Pore permeation coefficient}}{\text{Ideal gas flux (incident on a surface)}}$$

Some basic transport equations

Ideal gas flux.

$$J_{\text{ideal gas}} = \frac{\Delta P}{\sqrt{2\pi M R_u T}}$$

ΔP is the gas pressure, M is the molecular weight of the gas, R_u is the universal gas constant and T is the absolute temperature.

Permeation coefficient for viscous flow in pore. $\Pi = \pi R^4/\mu(3\pi R + 8L_p)$, where R is the pore radius, μ is the dynamic viscosity and L_p (0.535 nm for graphene) is the pore length (from ref. 102). Sampson's model: $\Pi = R^3/3\mu$; obtained for $L_p = 0$.

Ion conductance of pore.

$$G = \sigma\left(\frac{L_p}{\pi R^2} + \frac{1}{2R}\right)^{-1}$$

σ is the bulk ionic conductivity. This relation is valid for neutral pores.

Length scales

Graphene. Carbon atom van der Waals diameter: D_{vdw} = 3.4 Å. Carbon bond length in graphene: a = 1.42 Å. Area of a hexagonal ring in graphene is 5.24 Å^2.

Pore geometry. D_c is pore diameter defined by centres of edge atoms. $D_p \equiv D_c - D_{vdw}/\sqrt{2}$ is the pore diameter used for gas transport. $D_{p,vdw} = D_c - D_{vdw}$ is the pore diameter adjusted for van der Waals size of pore edge atoms, used for water/ion transport.

Gases. Kinetic diameter (Å): He (2.6), H_2O (2.65), H_2 (2.89), CO_2 (3.3), Ar (3.4), O_2 (3.46), N_2 (3.64), CH_4 (3.8), SF_6 (5.5).

Water molecule. Mean van der Waals diameter: 2.8 Å.

Ions. Diameter of hydrated ion (Å): Li^+ (7.64), Na^+ (7.16), K^+ (6.62), Mg^{2+} (8.56), Ca^{2+} (8.24), F^- (7.04), Cl^- (6.64), Br^- (6.60).

See Supplementary Section I for additional data, units and source references.

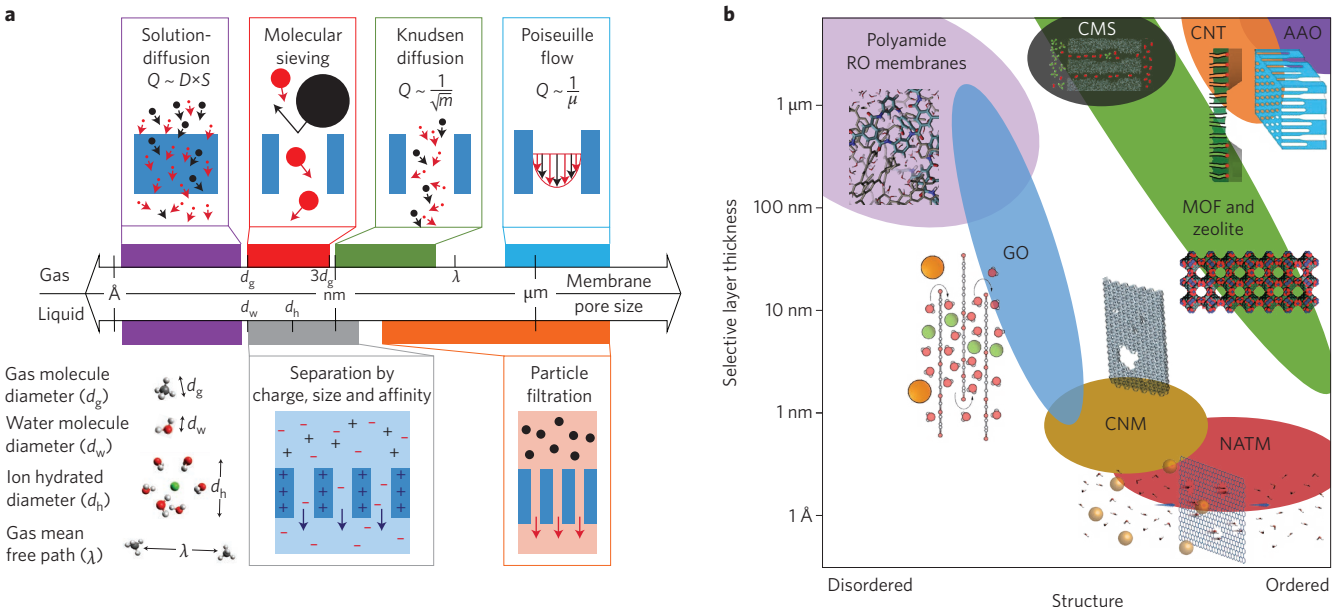

Figure 1 | Membrane characteristics and length scales. a, Length-scale dependence of membrane transport mechanisms. Relative scales of gas and water molecules, hydrated ions and gas mean free path are depicted on bottom left. Q, flux; D, diffusivity; S, sorption coefficient; m, molecular mass; μ, viscosity. **b**, Membrane structure–thickness map with some illustrative examples. From left to right, the structures change from disordered to ordered. Ideal NATMs are the thinnest with a high degree of order. Panel **b** images adapted from: ref. 193, Elsevier (polyamide reverse osmosis (RO) membranes); ref. 194, RSC (carbon molecular sieves (CMS)); ref. 21, AAAS (CNT); ref. 195, IOP (anodized aluminum oxide (AAO)); ref. 40, AAAS (graphene oxide (GO)); ref. 196, RSC (metal organic framework (MOF) and zeolite); ref. 197, American Chemical Society (carbon nanomembrane (CNM)); ref. 198, Macmillan Publishers Ltd (NATM).

is governed by diffusion alone (as in many polymeric gas separation membranes)[43], a more permeable material typically provides less selectivity and results in a trade-off between permeability and selectivity known as the Robeson limit in the context of gas separations[43,44]. Overcoming this trade-off requires incorporation of additional mechanisms such as chemical affinity or molecular sieving, where smaller molecules pass through while larger ones are sterically impeded (for example, in high free-volume polymers or carbon molecular sieves)[5,24,45].

Due to the small free volume available, gas transport in membranes with pore diameters just beyond the molecular size is governed by phenomena such as diffusion, surface adsorption and condensation of gas molecules in the membrane pores[24,43]. In pores that are much larger than molecular size but smaller than the gas mean free path, gas transport is governed by Knudsen diffusion[43,46], where molecules with lower molecular mass travel faster and have higher permeance. In liquid environments, transport in pores that are larger than molecules or ions is influenced by differences in species diffusivity, steric effects, chemical affinity and electrostatic interactions, including surface charge and dielectric effects[47].

Although transport in membranes is complex, a thin selective layer with precisely controlled pores and chemical functionality — which is potentially realizable with NATMs — is ideal for achieving high permeance and high selectivity (Fig. 1b). Realization of NATMs requires an understanding of gas- and liquid-phase transport across pores in atomically thin materials, which we now discuss.

Gas transport across atomically thin nanopores. In 2008, Bunch *et al.*[26] demonstrated that graphene is impermeable to helium and other gases, which opened the possibility of creating selectively permeable pores in graphene to realize selective membranes[26,48]. In their experiment, exfoliated pristine graphene 'nanoballoons' suspended over pressurized microcavities retained gases to within detection limits (Fig. 2a). This impermeability was attributed to the fact that pristine graphene does not have gas-permeable defects, the space between the carbon atoms in graphene is too small to allow for transport of gases and the contribution of quantum tunnelling is negligible[26].

A large number of theoretical studies[48–51] have explored the transport of different gases (for example, CH_4, CO_2, H_2, N_2, CO, H_2S, O_2, noble gases, alkanes and isotopes) through graphene and other NATMs with pore edges terminated with atoms including C, H, N, F and O (Fig. 2b) (see Supplementary Section II for a detailed list of references). The majority of these studies have focused on graphene and similar materials with inherent nanoporosity, such as porous graphene with various modifications[50,52–56], graphdiyne[57,58], graphyne[59] and two-dimensional (2D) polymers based on polypheneylene[60–62], porphyrin[63] and cyclohexa-*m*-phenylene[51]; exploration of other materials including hexagonal boron nitride (hBN)[64] has also begun.

These studies use one of two approaches to compute transport properties. (1) The energy barrier for a gas molecule to cross a pore is calculated using density functional theory (DFT)[51] or other quantum mechanical methods[50,62]; permeance is then estimated using a transition state approach given the gas molecule kinetic energy distribution[50], whereas selectivity is often estimated as the ratio of Arrhenius factors[51]. (2) The rate of molecules crossing the pore is calculated using classical (or first principles[48]) molecular dynamics simulations, which directly yields the permeance[49,56,65]. These studies have shed light on transport mechanisms[66,67], and revealed that permeance and selectivity can depend on differences in molecule size, mass, surface adsorption[68], interaction with functional groups on the pore rim, conformational entropy[54] and tunnelling rates[62,69,70].

To a good approximation, gas transport across atomically thin pores can be understood by comparing the diameters of the gas molecule (D_m) and the pore (D_p), though one needs to exercise caution as diameter definitions vary (Fig. 2d). When the pore is slightly larger than the gas molecule, gas transport is similar to effusion, that is, molecular flow across a thin aperture smaller than the gas mean free path, where the pore presents an effective area $A_{eff} \approx \pi/4(D_p - D_m)^2$ (see Box 1) that is smaller than the pore area $A_{pore} = (\pi/4)D_p^2$. Here, transport is dominated by steric considerations. When the pore size is approximately equal to or slightly smaller than the size of the gas molecule, the pore presents an energetic barrier to transport that depends on the molecule–pore repulsive interactions and any compliance due to bond stretching or flexing. We refer to this as the activated regime. If we assume a rigid pore with fixed atoms and approximate the molecule–pore interaction by the Lennard-Jones potential, the barrier height is given by

$$E \approx \frac{\pi D_c}{a} 4\varepsilon \left[\left(\frac{\sigma}{D_c/2} \right)^{12} - \left(\frac{\sigma}{D_c/2} \right)^{6} \right] \approx \frac{4\pi\varepsilon D_c}{a} \left(\frac{\sigma}{D_c/2} \right)^{12}$$

where ε and σ are the Lennard-Jones parameters, $D_c/2$ is the distance from the pore centre to the centre of the atoms constituting the pore, a is the distance between adjacent atoms on the pore rim and $\pi D_c/a$ gives the average number of atoms on the pore rim (Fig. 2d). Assuming that all gas molecules with kinetic energies exceeding this value cross the pore, we obtain an Arrhenius-like expression for the effective pore size

$$\frac{A_{eff}}{A_{pore}} \approx \frac{1}{2} \operatorname{erfc}\left(\sqrt{\frac{E}{k_B T}} \right)$$

where k_BT is the Boltzmann factor (see Box 1 and Supplementary Section IV).

The effective pore areas predicted from simulations for different gas molecules across pores with different structures and functional groups, compiled from 33 literature reports, agree with this model and indeed collapse into two regimes (Fig. 2e)[48–59,61,63–65,68,69,71–85]. The steric regime has a high A_{eff} and a high permeation coefficient, with $0.0025 \lesssim A_{eff}/A_{pore} < 1$ and $\pi/4(D_p - D_m)^2 \gtrsim 0.24$ Å^2. A_{eff} and the permeation coefficient decrease rapidly in the activated regime as the pore size is reduced below the molecule size. For the majority (~75%) of simulated pores, effective pore areas and the corresponding permeation coefficients (see Box 1) of the most permeable molecule range from 10^{-4}–10 Å^2 and 10^{-23}–10^{-19} mol s^{-1} Pa^{-1}, respectively, which, for a pore density of 10^{12} cm^{-2}, corresponds to a membrane permeance of 10^{-7}–10^{-3} mol m^{-2} s^{-1} Pa^{-1} (10^2–10^6 GPU). For example, graphene pores with diameters of 3.6 and 4.8 Å were reported to present effective areas of 9.9×10^{-3} and 5.2 Å^2 (effective diameters of 0.11 and 2.57 Å), permeation coefficients of 1.8×10^{-23} and 9.3×10^{-21} mol s^{-1} Pa^{-1} and permeance of 5.3×10^2 and 2.8×10^5 GPU, respectively, to hydrogen[75,81] (kinetic diameter 2.89 Å) (see Supplementary Section I for equations relating these parameters). However, some simulations involve pore densities of up to 8.5×10^{14} cm^{-2}, resulting in permeances up to 10^{-1} mol m^{-2} s^{-1} Pa^{-1} (10^8 GPU).

Given two different gas molecules, there are three possible regimes depending on pore size (Fig. 2d). (1) For large pores, transport is in the steric regime for both molecules and high selectivity is not possible. (2) Selectivity by molecular sieving accompanied by high permeance occurs when the pore size lies in between the sizes of the two gas molecules; transport of the smaller molecule is in the steric regime while that of the larger one is in the activated regime. (3) High selectivity at very low permeance occurs for small pores when transport of both molecules is in the activated regime. Interestingly, this simple steric exclusion and activated transport model predicts a trade-off between permeance and selectivity, analogous to the Robeson limit, and is consistent with published reports from theoretical studies (Figs 2f and 5f); smaller pore sizes lead to higher selectivity and lower permeance due to the highly nonlinear dependence of the energy barrier on pore size.

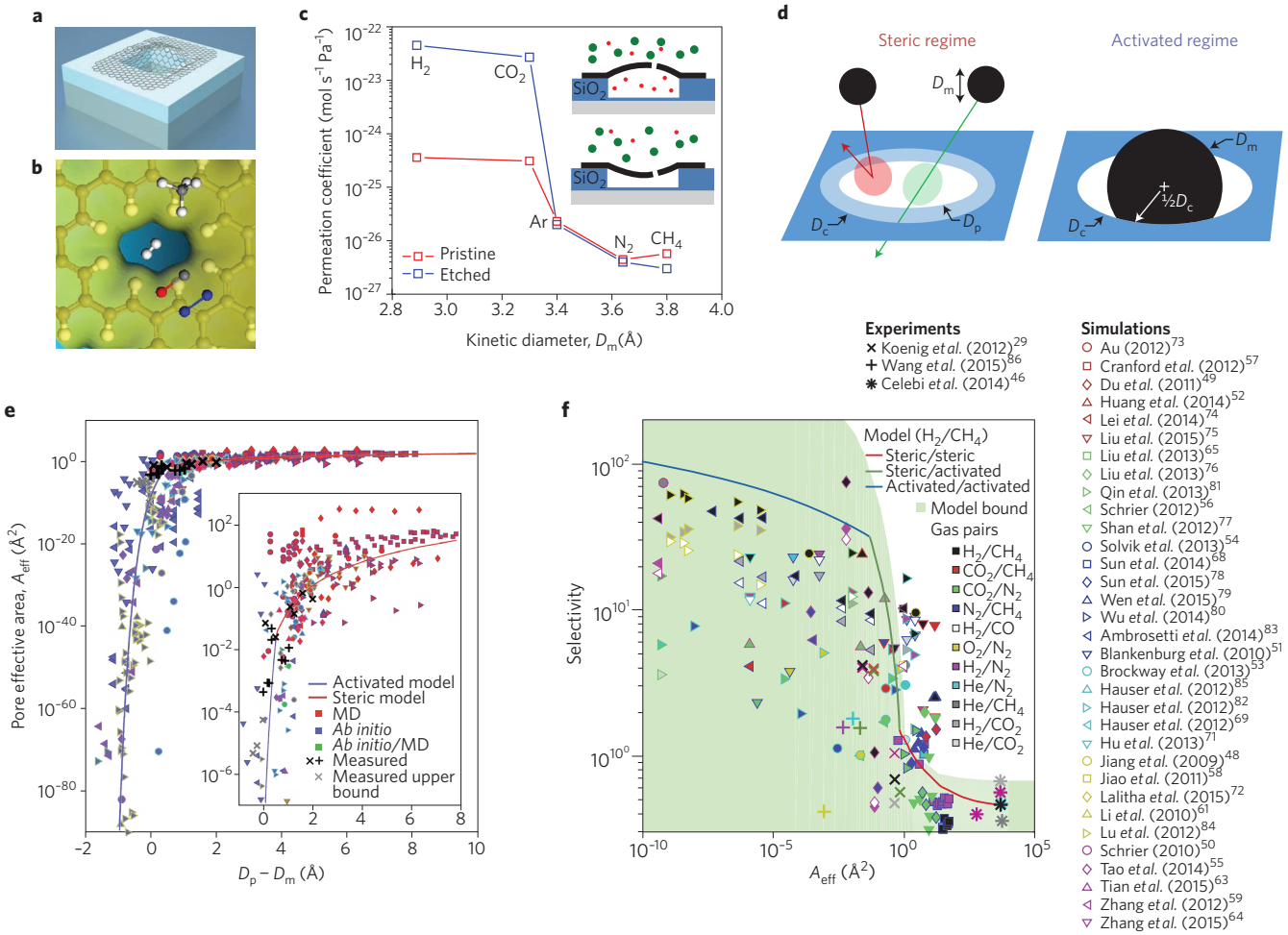

Figure 2 | Gas transport across NATM pores. a, Schematic of a graphene nanoballoon experiment[26] in which graphene suspended over a cavity retained pressurized helium. **b**, Visualization from simulations[55] of a hydrogen-functionalized graphene pore along with H_2, N_2, CO and CH_4 molecules. H, C, N and O atoms are shown in white, grey, blue and red, respectively, and the 0.02 Å^{-3} electron density isosurface is shown in yellow. **c**, Permeation coefficient of pristine and ultraviolet/ozone etched bilayer graphene measured in ref. 29 showing molecular sieving through a graphene nanopore, with H_2 and CO_2 preferentially effusing through the etched graphene. Inset: small gas molecules (in red) escape through the selective pore while big molecules (in green) cannot enter, leading to a measurable membrane deflection. **d**, Illustration of transport model and mechanism of steric/activated gas transport. Carbon centres located at D_c with pore diameter defined as $D_p = D_c - D_{vdw}/\sqrt{2}$, where D_{vdw} is the van der Waals diameter of a carbon atom. **e**,**f**, Compilation of simulation and experimental data of gas flow through NATM pores for different gas molecules and pore sizes qualitatively agrees with scaling model and illustrates the steric/activated transport regimes (see Supplementary Section III for data extraction and Supplementary Section IV for scaling model). Marker border colour indicates the source. **e**, Pore effective area decreases sharply when the pore size falls below the molecule size. Marker fill colour indicates the simulation method used. 'Measured upper bound' indicates an experimentally measured upper bound on permeance, where the flow rate through the graphene pore was below the measurement resolution. '*Ab initio* / MD' indicates that the reported effective area is based on a permeance (for gas B), which was computed as the ratio of the permeance of a more permeable gas species (gas A), determined by classical molecular dynamics (MD), and the selectivity (A/B), determined by *ab initio* calculations. **f**, Selectivity versus effective pore area. For clarity, the curve predicted by the model is shown for H_2/CH_4 since curves for other gas pairs (shown in Fig. S3) are qualitatively similar. Marker fill colour identifies the gas pair. Shaded area bounds the model predictions for all gas pairs. Note the double-log scale on the *y* axis. Panels adapted from: **a**, ref. 26, American Chemical Society; **b**, ref. 55, American Chemical Society; **c**, ref. 29, Macmillan Publishers Ltd.

Molecular dynamics tends to better resolve high permeance, but has difficulty quantifying high selectivities ($\gtrsim 10^3$) because of the limited number of observable molecule crossings imposed by a limited simulation time ($\lesssim$100 ns). DFT-based approaches can resolve higher selectivities with reported values ranging up to 10^{78}, but some of these correspond to impractically low permeance.

Although the above model captures the basic dependence of permeance and selectivity on molecule size, other phenomena can determine selectivity when differences in size are not sufficiently large to be the determining factor. For example, permeance of gas molecules may be enhanced by adsorption and surface diffusion of the gas molecules towards the pore[67] or by interactions with partial charges on the pore edge. In porous graphene, permeance is enhanced in the order (1) SO_2 (ref. 60) > CO_2 (refs 56,60,77) > CH_4 (refs 56,60,68) > H_2O (ref. 60) > N_2 (refs 49,56,60,68,77,79) / O_2 (refs 56,60) > H_2 (refs 49,68,79) > He (ref. 68) (permeance enhancements in the case of N_2 and O_2 are comparable); (2) H_2S (ref. 60) > CH_4; and (3) paraffins > olefins[54]. Similar effects have been reported for variations of porous graphene[54,56] and 2D polyphenylene[60], and are also implicated in enhanced CO_2 transport in graphene oxide membranes[32]. Entropic barriers arising from constrained conformations of molecules passing through the pore can lead to selective transport of shorter hydrocarbon molecules compared with longer ones[54]. Quantum tunnelling can dominate

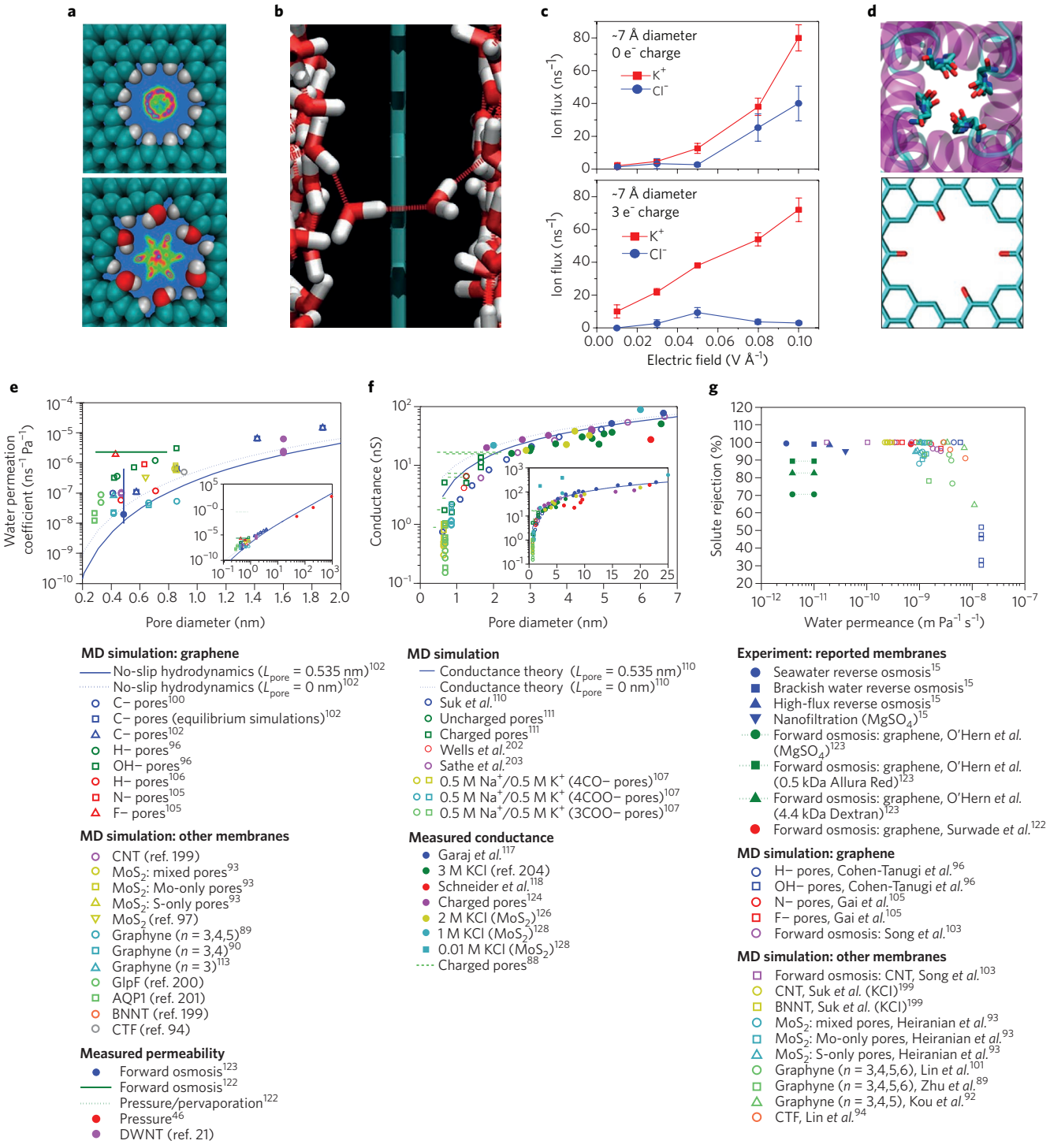

Figure 3 | Water and ion transport across NATM pores. a, Preferential configurations adopted by water molecules traversing hydrogen or hydroxyl terminated graphene pores[96] are illustrated by water-oxygen density maps. Red denotes high density. **b**, Single-file water transport in a graphene pore[100]. **c**, Nonlinear increase in ion flux with electric field illustrates the ion dehydration barrier. Addition of a negative pore charge enhances the flux of K^+ while suppressing Cl^- flux (from ref. 111). **d**, Illustration of a C=O terminated graphene pore designed to mimic a KcsA potassium ion channel (from ref. 107). **e**, Compiled data of simulated and experimentally measured water permeation coefficients show increase with pore diameter consistent with continuum theory (see Box 1). 3CO, 3COO, and 4COO denote pores terminated by 3 carbonyl and 3 or 4 carboxylate groups, respectively. **f**, Compiled data of simulated and experimentally measured ionic conductance for electrically driven transport of KCl compare well with continuum theory (see Box 1). Conductance is scaled to 1 M KCl (see Supplementary Section V). Estimated pore diameters are reported in refs 88,124. **g**, Compiled data of simulated and experimentally measured solute rejection and water permeance with respect to reported NATM membrane area, compared with that of commercial membranes from ref. 15. Solute is NaCl unless otherwise noted. In **e**–**g**, open markers are from molecular dynamics (MD) simulations, filled markers are for experimentally measured values, and horizontal solid or dashed lines indicate the estimated range for experimentally measured values. GlpF, aquaglyceroporin; AQP1, aquaporin 1; BNNT, boron nitride nanotube; CTF, covalent triazine framework; DWNT, double-walled carbon nanotube. Panels adapted from: **a**, ref. 96, American Chemical Society; **b**, ref. 100, American Chemical Society; **c**, ref. 111, AIP; **d**, ref. 107, American Chemical Society.

transport[62,69,70] at low temperatures where the kinetic energy of gas molecules is much smaller than the energy barrier, which has been proposed for separating helium isotopes[69].

Experimental evidence of molecular sieving through NATMs was first reported in 2012 by Koenig *et al.*[29] (Fig. 2c). Gas permeance of initially impermeable bilayer graphene nanoballoon membranes was monitored as nanopores were created in the graphene by ultraviolet/ozone etching, where a single pore is likely to dominate transport[86]. One graphene membrane permitted selective transport of H_2 and CO_2 over the larger Ar, N_2 and CH_4 molecules (~3.4 Å pore) (Fig. 2c) and another membrane permitted transport of the above molecules but not that of larger SF_6 (~4.9 Å pore), with observed selectivities exceeding 10,000 (ref. 29). In subsequent studies with a single-layer graphene membrane, permeance was observed to decrease with increasing kinetic diameter for He, Ne, H_2 and Ar, but was anomalously high for N_2O and CO_2 (ref. 86), consistent with flux enhancement due to polar interactions[56,60,77]. The permeation coefficients in these experiments were in the range of 10^{-23}–10^{-21} mol s^{-1} Pa^{-1} (pore effective area 5×10^{-3}–0.4 $Å^2$) in reasonable agreement with theoretical studies (Fig. 2e,f).

Although experimentally measured gas permeance generally agreed with simulations, transport through single-layer graphene pores was observed to fluctuate on a timescale of minutes, which was postulated to originate from thermally activated rearrangement of molecular bonds at the pore[86,87]. Similar observations in multiple pores[86] and in liquid environments[88] suggest that dynamic fluctuations in transport across NATM pores may be common, although understanding their origin remains elusive. This also highlights the need for more controlled experiments and more realistic simulations that complement those on idealized model pores. For example, the majority of simulations fix the 2D lattice or the position and orientation of the gas molecules in calculating the energy barrier, although some studies take these into account[52,56,64,68,73,78,79,82,83]. DFT calculations that permit lattice deformation[82] or molecular dynamics simulations using the adaptive intermolecular reactive empirical bond order (AIREBO) potential that allows for deformation and thermal fluctuations[56,68,73,78,79] indicate that assuming a fixed lattice can greatly over-predict selectivities[79,82].

Gas transport in larger pores is less complicated, but permeance is still very high owing to the atomic thickness of the membrane. Celebi *et al.*[46] showed that graphene bilayer membranes with an array of 7.6-nm-diameter pores machined by a focused ion beam exhibited H_2/CO_2 selectivity consistent with effusion, but had more than three orders of magnitude higher permeance (~10^{-2} mol m^{-2} s^{-1} Pa^{-1}, based on graphene area) than existing gas separation membranes with similar selectivity. Gas flow followed free-molecular effusion theory for small pores (≲50 nm) and a modified Sampson's model (Box 1) for large pores.

Water and ion transport across atomically thin nanopores. Motivated by applications in water desalination and purification, theoretical studies using classical molecular dynamics (or other methods[89–91]) have focused on transport of water and ions driven by pressure[89,90,92–102], osmosis[103–106] and electric fields[107–111] across graphene with different pore terminations (C (refs 95,100,102,110,111), H (refs 96,98,99,103,106,109,112), hydroxyl[95,96,103,106], carbonyl[107], carboxyl[95,106,107], amine[95], F (refs 99,103,105,109), N (refs 105,109), O (ref. 108)), variants of graphyne[89–92,101,104,113,114], MoS_2 (refs 93,97) and covalent organic frameworks[94].

Transport of water molecules (~2.8 Å van der Waals diameter) through NATM pores is largely determined by pore size. Graphyne-2 pores with ~2.9 Å diameter present a small barrier to water transport[91]; pores larger than ~3 Å (which corresponds to atom centre-to-centre diameters, D_c, of ~6 Å) easily permit transport of water[95,103,105]. When the pore size is below ~2 nm, transport of water is also influenced by hydrogen bonding and structuring of water molecules, which depends on the pore geometry and functional groups[95,96,98,100,102,103,105,112,115]. The smallest pores in graphene[95,100,102,103], graphyne[89,90,113] and MoS_2[93] that permit water transport can accommodate only a single water molecule in their cross-section and therefore exhibit single-file movement of water molecules. In pores with diameter ≲1.5 nm (ref. 112), water molecules adopt certain preferential configurations as they pass through the pores[95,101,112] (Fig. 3a,b); similar effects are also observed in other nanoscale conduits such as CNTs[116]. In NATM pores, a significant fraction of the pressure drop occurs in the entrance and exit regions outside the pore[102]. As, in many cases, entrance and exit resistance dominates transport in CNTs, flow rates through NATM pores are comparable to those in CNTs of similar diameter[100,102,113] (Fig. 3e). These flow rates are, in fact, predicted reasonably accurately (within an order of magnitude) by continuum no-slip hydrodynamics (see Box 1) for NATM pores[102]. Flow enhancement is observed in molybdenum-terminated MoS_2 pores that mimic the conical shape of biological aquaporin channels and reduce the flow resistance at the entrance and exit[93]. The effect of pore functional groups on water flow tends to be modest, with hydrophilic groups (for example, –OH, Mo, –N) reported to enhance permeation of water by up to twofold[93,94,96,99,105,106] by attracting water molecules to the pore, compared with hydrophobic groups (for example, –H), which can present an entropic barrier to transport[96].

Transport of hydrated ions across atomically thin pores is influenced by electrostatic interactions, coordination with functional groups or charges at pore edges, and steric exclusion of the ion hydration shell[37,96,105,109–111] (Fig. 3c,d,f). The diameters of the first hydration shell for Na^+, K^+ and Cl^- are ~6.6–7.2 Å, which require pore diameters exceeding ~7 Å (D_c exceeding ~10 Å) for ions to pass through with an intact hydration shell[95]. Neutrally charged pores smaller than the ion hydration size therefore present a barrier to ion transport that depends on the energy required for dehydration and the electric polarizability of the NATM material[47]. For example, Zhao *et al.*[111] observed that 4-Å-diameter neutrally charged graphene pores completely excluded both K^+ and Cl^-, but 8 Å pores permitted passage of both ions. Ionic transport across larger, neutral pores is dominated by the 'access resistance' associated with the pore entrance and exit that is approximated well by continuum theory[110] (Box 1 and Fig. 3f).

Pore functionalization can radically alter ionic transport, especially if the pore is smaller than the size of the hydrated ion. Charged or partially charged functional groups along the pore edge can lower the energy barrier for ions of opposite charge and increase the barrier for ions of like charge[95], leading to cation/anion selectivity. For example, Sint *et al.*[109] showed that a ~5-Å-diameter graphene pore could be made cation selective by functionalizing the pore with electronegative F or N atoms. Similarly, Zhao *et al.*[111] observed that negatively charged, 4-Å- and 8-Å-diameter graphene pores permitted selective transport of K^+, but the ionic flux increased nonlinearly with voltage as higher voltages facilitated partial dehydration of the K^+ ion (Fig. 3c). Counterintuitively, by partially shedding their hydration shells, larger ions with lower hydration energies traverse pores more easily than smaller ions with tightly bound hydration shells[109]. Ion transport can also drive fluid flow under an applied potential difference[111], a phenomenon called electroosmosis that finds use in fluidic pumping. Functionalized atomically thin pores that structurally resemble biological ion channels (Fig. 3d) show some similar behaviours, such as voltage gating and cation/cation selectivity[107,108], although the pores are much thinner than their biological counterparts. This raises the intriguing question as to what extent atomically thin pores can be tailored to achieve high ion selectivity, voltage sensitivity and other functionalities of biological channels.

The smaller size of water molecules compared with that of hydrated ions enables their separation when NATM pores are large enough to pass water, but small enough to block hydrated ions (Fig. 3g). Cohen-Tanugi and Grossman[96] demonstrated rejection of Na^+ and

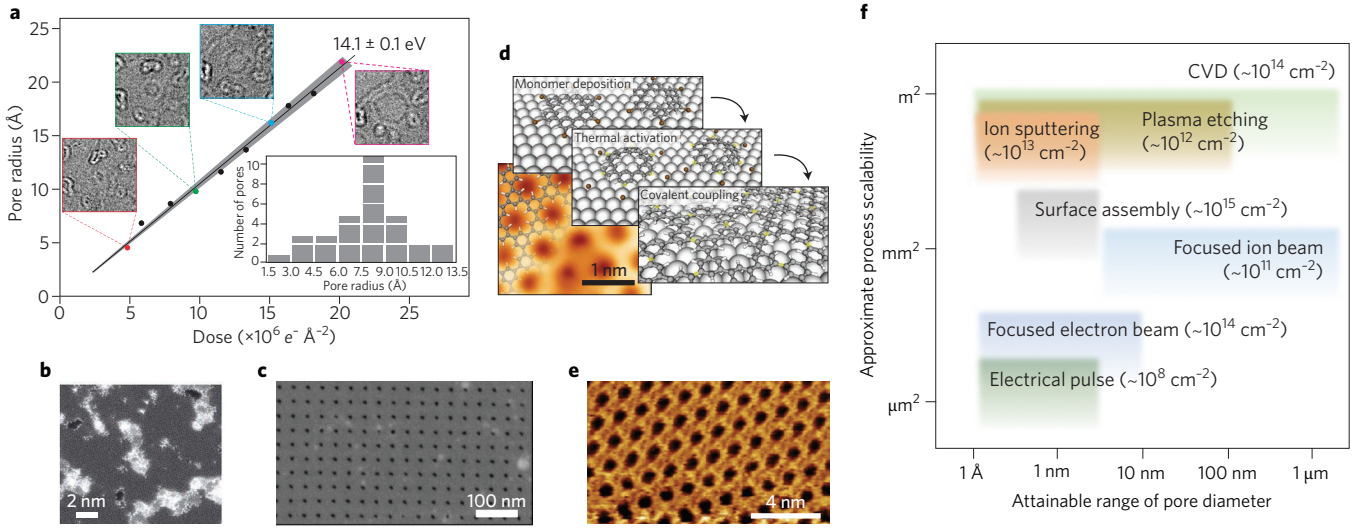

Figure 4 | NATM pore creation methods. a, Electron irradiation-mediated growth of pores in graphene nucleated by argon ion bombardment. Inset depicts a pore size distribution[145]. **b**,**c**, Electron microscopy images of pores in single-layer graphene created by oxygen plasma[122] and focused ion beam machining[46], respectively. **d**,**e**, Scanning transmission electron microscopy images and schematics of bottom-up synthesis of porous 2D polymers by self-assembly on a Ag(111) surface[51] and at an air/water interface[170], respectively. **f**, Pore diameter versus approximate upper bound of membrane area that can be fabricated using different pore creation methods. Numbers in parentheses represent estimates of the highest possible pore density at the smallest possible pore size for each method. Panels adapted from: **a**, ref. 145, PNAS; **b**, ref. 122, Macmillan Publishers Ltd; **c**, ref. 46, AAAS; **e**, ref. 170, American Chemical Society. Panel **d** reproduced from ref. 51, Wiley.

Cl^- ions for hydrogen- and hydroxyl-terminated graphene pores with diameters below 5.5 Å, even at realistic operating pressures for reverse osmosis (10–100 bar)[98]. Heiranian *et al.*[93] showed that MoS_2 pores below 6 Å could reject NaCl while supporting high water flux. Pressure-driven separation has also been shown for trihalomethanes in 6 Å graphene pores[99], NaCl in graphyne-3 (~4 Å)[89,90,92,101], NaCl in graphyne-4 (~6 Å) with a fixed lattice[89] (<100% rejection[90,92,101,104] with a non-fixed lattice), $CuSO_4$, benzene and CCl_4 in graphyne-3 (ref. 101), and Mg^{++}, Ca^{++}, K^+, Na^+ and Cl^- in graphyne-3 and variants[90]. Rejection of NaCl has also been demonstrated in forward osmosis in graphene[103,105,106] and graphyne-3[104], consistent with selectivity governed by size effects. Compiled results indicate the theoretically predicted potential for high solute rejection and permeance of NATMs compared with existing membranes, although this performance remains to be experimentally realized (Fig. 3g).

A few experimental studies have probed transport across atomically thin pores[46,117–129], with particular focus on electrically driven ionic transport across pores in graphene[117–119,124], hBN[125] and MoS_2 (ref. 126), motivated by applications in DNA analysis. Ionic conductance of large pores (>2 nm) in graphene and MoS_2 agrees reasonably well with continuum descriptions of ion transport[110,117,124,126,127], although a surprisingly high K^+/Cl^- selectivity was recently observed in large (20 nm) graphene pores, which was attributed to the surface charge on graphene[124]. Experimental data on the behaviour of smaller pores (≤2nm) is limited (Fig. 3f). Hints of ion transport through subnanometre pore defects[109,110] smaller than the ion hydration shell were first seen in a study by Garaj *et al.*[117], who observed that salts of larger monovalent ions with lower hydration energies displayed higher conductance than salts of smaller ions. Jain *et al.*[88] attempted to isolate pore defects by suspending graphene across a silicon nitride nanopore. They observed linear, rectified and nonlinear current–voltage characteristics consistent with ion dehydration and electrostatic effects in subnanometre pores. Their observation of cation/cation selectivity and voltage-activated fluctuations[88] also hints at parallels between atomically thin nanopores and biological ion channels[107,108]. Nonlinear current–voltage characteristics, effects of charge quantization and high ionic current density driven by salt concentration difference were recently observed in MoS_2 nanopores[128,129], which may find use in energy harvesting from salinity gradients.

Ionic selectivity in macroscale single-layer graphene membranes was reported by O'Hern *et al.*[121], who introduced subnanometre pores in graphene by ion bombardment followed by chemical etching. Although there was significant leakage through defects, the membranes exhibited some K^+/Cl^- selectivity consistent with electrostatic exclusion of Cl^- due to negatively charged pore functional groups[111] expected in oxidative etching; with further etching, the membrane permitted selective transport of KCl over a larger organic molecule (~1.0 nm size). Osmosis-driven water flux measured across similar graphene membranes with ~0.5 nm pores[123] was consistent with molecular dynamics predictions by Suk and Aluru[102]. Water/ion selectivity was demonstrated by Surwade *et al.*[122] using oxygen plasma to introduce ~1 nm pores at a density of ~10^{12} cm^{-2} in single-layer graphene placed on a micrometre-scale aperture. For a certain plasma treatment, all NaCl ions were rejected and water permeated at high rates, though only one side of the membrane was wetted and evaporation may have played a role. Water transport has also been measured across larger (50–1,000 nm) pores in bilayer graphene, with results consistent with continuum theory[46]. Although a picture of water and ion transport across atomically thin pores is beginning to emerge, experimental data are sparse, there are some discrepancies among the simulation results and ion selectivity remains to be understood (Fig. 3f).

Compared with water or ions, protons show distinct transport behaviours. Geim and co-workers discovered that monolayers of (nonporous) pristine graphene and hBN are permeable to protons[130] and have high selectivity (~10) over deuterons[131], opening new possibilities for deuterium/hydrogen separation. The observation that small, otherwise impermeable defects in graphene could also permit selective proton transport[132,133] suggests the possibility of creating high-permeance proton-selective NATMs from materials such as graphyne-1.

Fabrication of NATMs

Practical realization of NATMs requires synthesis of a continuous layer of atomically thin material with controlled porosity as well as

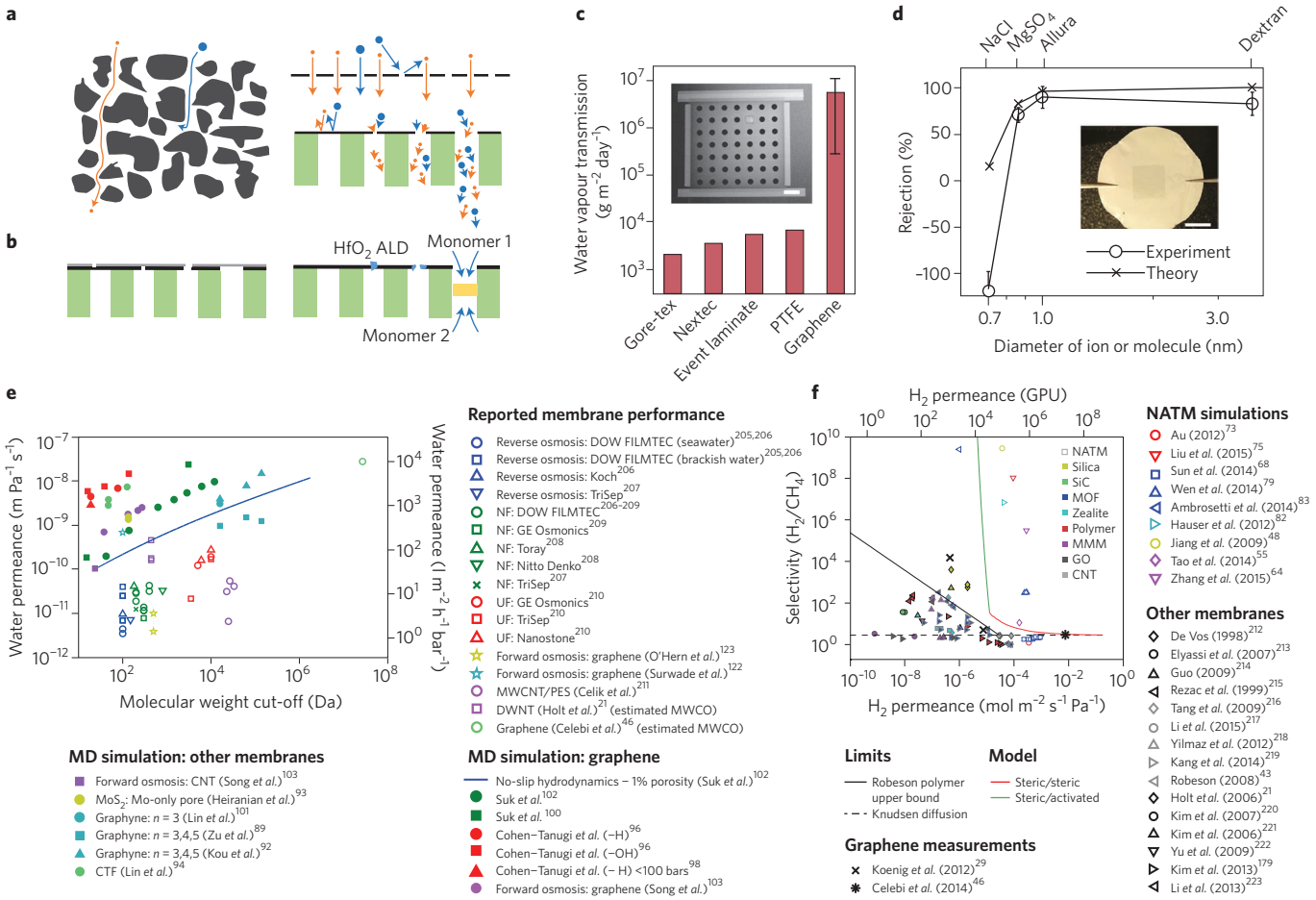

Figure 5 | Transport characteristics of NATMs. a, Pathways for transport of molecules of different sizes across membranes with torturous pores (left) and unsupported and supported NATMs (right). **b**, Schematics of defect sealing in NATMs. Left: stacking of multiple layers. Right: sealing of small defects using atomic layer deposition (ALD) of hafnia, and of large defects by reaction of monomers that form plugs only at defects[123]. **c**, Fast water vapour permeation across NATMs with 400 nm pores formed by focused ion beam milling in two-layer graphene[46]. PTFE, Polytetrafluoroethylene. The inset shows a membrane comprising freestanding circular areas of graphene into which pores are drilled. Scale bar, 10 μm. **d**, Forward osmosis-driven nanofiltration across single-layer graphene membranes (inset) with sealed defects. Results are compared with continuum theory assuming only size exclusion[123]. Scale bar, 0.5 cm. **e**, Compilation of simulation and experimental water permeance data versus estimated molecular weight cut-off across NATMs compared with a few other illustrative membranes. **f**, Compilation of simulation and experimental selectivity–permeance data for H_2/CH_4 separation across NATMs compared with a few other membranes. In **e**,**f**, permeability data for membrane materials were converted to permeance assuming a 100-nm-thick selective layer. NATMs without inherent porosity, such as graphene, were assumed to have a pore density of 10^{12} cm^{-2}. NATMs with inherent porosity had pore densities of up to 8.5×10^{14} cm^{-2}. CTF, covalent triazine framework; NF, nanofiltration; UF, ultrafiltration; MWCNT/PES, multi-walled carbon nanotube/polyethersulfone; DWNT, double-walled carbon nanotube; MWCO, molecular weight cut-off; MMM, mixed-matrix membrane; GO, graphene oxide. Panel **c** reproduced from ref. 46, AAAS. Panel **d** adapted from ref. 123, American Chemical Society.

the ability to handle the materials using suitable porous supports. NATMs can be fabricated 'top-down' by creating pores in an initially nonporous atomically thin material, or by 'bottom-up' synthesis of an intrinsically porous material.

Top-down fabrication. Chemical vapour deposition (CVD) has emerged as a tunable and versatile method for producing continuous layers of 2D materials over large areas[134] and lends itself easily to fabrication of NATMs. Within a year of the first demonstration of large-area CVD growth of monolayer graphene on copper by Li *et al.*[135] in 2009, Samsung demonstrated roll-to-roll transfer of 30-inch sheets of CVD graphene[136], and SONY later demonstrated roll-to-roll synthesis and transfer to produce 100-m-long graphene-coated films[137]. Several methods are now available to handle and transfer graphene and other 2D materials to various substrates[138], and membranes have been made without transfer by introducing pores in the catalytic substrate before[139] or after[140] CVD growth. Besides CVD methods, mechanical exfoliation of 2D layered materials produces thin, pristine flakes that are ideally suited for physics experiments or microscale membranes[29], whereas liquid-phase exfoliated 2D materials[134] are less suitable due to the need to assemble and fill in gaps between flakes. Experimental work on NATMs has therefore largely focused on exfoliated and CVD graphene, for which technical know-how is most advanced.

Subnanometre pores can be introduced in the initially nonporous material by 'top-down' approaches using ion irradiation[121,141–147] or chemical/plasma etching[29,86,122,148–152] (Fig. 4a–c). Etchant chemistry dictates the pore functional groups and can stabilize the pores[153], whereas pore density and size depend on the interplay between nucleation of defects and their growth into larger pores[154]. For example, thermal oxidation of graphene or graphite in oxygen produces a low (<10^{10} cm^{-2}) density of large (>10 nm) holes[155], while ozone tends to easily nucleate defects to yield a high density of pores[154,156]

and was used for creating gas-selective pores in graphene nanoballoons[29,86]. Oxygen plasma can also induce[148,149] and grow nanometre-scale pores in suspended single-layer graphene[122,151] at a high density (~10^{12} cm^{-2}, Fig. 4b). Nucleation of defects followed by growth can produce more uniform pores with controllable size and density[146]. This was realized in graphene using oxygen and hydrogen plasma, respectively, to nucleate and grow pores[149]. Ion irradiation can also controllably nucleate defects, which can be followed by electron-induced sputtering or chemical etching to create a high density (~10^{12}–10^{13} cm^{-2}) of subnanometre pores[121,123,145] (Fig. 4a). Ion angle of incidence, energy and type determine the kind of defect, whereas the ion fluence determines their density[141,142]. An energy threshold of ~30 eV is required to produce defects in graphene[157], indicating that ion impact could also play a role in plasma treatment[146]. Whereas these methods produce a distribution of pore sizes[121,145] and perhaps work well only in single-layer materials, focused ion beams can precisely machine a large number of individual pores down to ~8 nm in diameter[46] (Fig. 4c). Electron beams focused below 1 nm can create precise subnanometre to few-nanometre pores[117,158,159]. Other methods to create pores include the use of block copolymers[160] or substrates[161] as templates, reduction of graphene oxide[162], catalyst-induced etching[163,164], electrochemical machining by atomic force microscopy[86], or the use of electrical pulses to create pores with subnanometre accuracy in graphene[127] or MoS_2 (ref. 165).

Bottom-up fabrication. In contrast to the creation of pores in an initially nonporous material, recent advances in the synthesis of intrinsically porous covalently cross-linked single or few-layer 2D polymers[166,167], including graphyne and its variants[168], have potential for creating a high density of atomically precise pores tailor-made for specific applications, directly in a covalently bonded single layer[51,59,90,94,101,113]. For example, surface-assisted synthesis of nanoporous graphene by aryl–aryl coupling of polyphenylene-based precursors or cyclodehydrogenation using polycyclic aromatic hydrocarbons has been proposed[51] (Fig. 4d). Graphdiyne has been synthesized at the millimetre scale by cross-linking of hexaethynylbenzene on copper under nitrogen atmosphere[169], which may permit selective transport of hydrogen[59], and possibly water[91] or protons. Recently, a 2D polymer with ~0.8 nm pores was synthesized by ultraviolet cross-linking of triptycene-based amphiphilic monomers self-assembled at the water/air interface in a Langmuir–Blodgett trough[170] (Fig. 4e). The high quality of the resulting polymer and the ability to transfer centimetre-scale areas to porous supports makes it a promising route to realize NATMs.

Another potential route to NATM fabrication is by modifying synthesis processes that normally result in nonporous materials. Pores could potentially be created in a modified CVD process by controlling the ratio of the growth precursor and etchant (for example, CH_4 and H_2 for graphene)[171], introducing etchants during or post synthesis, templating of the catalytic substrate[161] or substitutional doping to generate precisely defined pores[172]. However, atomic precision and high porosity may be difficult to realize with these approaches.

Scalability, quality and stability. Among the top-down methods, pore creation in CVD-grown materials by chemical and plasma routes is amenable to fabrication of large-area NATMs (Fig. 4f). Machining using focused ion beams is less scalable and appropriate for smaller membranes, whereas electrochemical methods and machining using atomic force microscopy or tightly focused electron beams are suitable for creation of a few pores for microscale membranes. Bottom-up approaches remain relatively unexplored for membrane applications, and key challenges are to engineer practical processes for synthesis of continuous layers over sufficiently large areas[167]. As of now, roll-to-roll processed 2D materials are not commercially available, and CVD-grown materials remain inherently polycrystalline with intrinsic vacancy defects, grain boundaries and wrinkles that contribute to leakage pathways[120,173]. Compared with applications in electronics, the quality requirements for atomically thin materials for membrane applications are more stringent in some respects, as small pinhole defects can severely compromise selectivity. To address these issues, synthesis processes need to be tailored to minimize pinhole defects, and methods to assess quality for membrane applications need to be developed. In addition, polymer-based methods to transfer atomically thin materials tend to leave surface contamination, the effects of which on transport across the membrane are poorly understood. Techniques for clean transfer and control of surface contamination are also essential to ensure quality and reproducibility.

Mechanical stability of NATMs is essential to withstand handling, abrasion and high pressures. Graphene has a remarkably high fracture strength of 130 GPa (~44 N m^{-1}) and tolerates strains of ~25% (ref. 27), which would facilitate its handling on a support. Although pores and defects can decrease the fracture strength by about an order of magnitude[151,174], it is more than sufficient to withstand high pressures when the atomically thin layer is properly supported. The ability to withstand pressure scales inversely with the support pore diameter, and molecular dynamics simulations indicate that nanoporous graphene can withstand a pressure of 570 bar when suspended over 1 μm pores[175]. Sufficiently high strengths are also expected of other atomically thin materials including MoS_2 (ref. 176), graphyne[89,101] and covalent organic frameworks[94]. Adhesion and abrasion resistance are other important considerations related to slippage, delamination and wear of NATMs. Graphene exhibits a high adhesion energy[177] and good abrasion resistance[178], but abrasion resistance in the context of membranes is not well understood and protective coatings will be required if the atomically thin layer is damaged easily. Similarly, although NATMs are expected to be chemically stable[28,152], studies that specifically investigate this aspect are needed.

From pores to membranes. Provided that transport across a pore is not influenced by its neighbours, the net flux across NATMs is the sum of those across the membrane pores. Using this assumption, the predicted permeance ranges from 10^4 to 10^8 GPU and exceeds 1,000 l m^{-2} h^{-1} bar^{-1} for gas separations and water desalination, respectively, significantly surpassing the permeance of polymeric membranes (Fig. 5e,f). These estimates constitute upper bounds, since real membranes will inevitably have a distribution of pore sizes and defects that are situated in parallel with each other (Fig. 5a). NATMs are therefore extremely sensitive to leakage through defects, and their size selectivity is determined by the largest pores[123] — presenting a major engineering challenge that may well turn out to be the Achilles heel for some applications. It is for this reason that only a few studies have demonstrated selective transport across non-microscopic NATMs, which requires strategies to minimize the impact of defects by independent stacking of layers[46,173], sealing of defects[123], appropriate choice of the porous support[173] or other mechanisms[131] (Fig. 5b).

Celebi *et al.*[46] stacked two layers of graphene on a silicon support to form a nearly impermeable layer, into which ordered arrays of pores with diameters of 8–1,000 nm were machined using a focused ion beam. The measured water flow rates (per unit graphene area) were five- to sevenfold greater than commercial ultrafiltration membranes, whereas vapour transport rates were two to three orders of magnitude higher than those in commercial membranes (Fig. 5c). Boutilier *et al.*[173] showed that gas transport through stacked graphene layers can be explained by random alignment of defects, resulting in exponential decrease in gas permeance with selectivity approaching the Knudsen limit. Kim *et al.*[179] stacked five layers of graphene on a polymeric membrane to enhance its barrier properties. The O_2/N_2 selectivity exceeded the Knudsen limit, and was attributed to defects and inter-layer transport. Although there are no reports of creating aligned subnanometre pores in multilayer materials, the stacking approach may be useful for materials like graphyne that have high intrinsic porosity.

O'Hern *et al.*[123] created centimetre-scale single-layer graphene NATMs by multiscale sealing of defects. Nanoscale defects were sealed by atomic layer deposition, which tends to deposit preferentially on defects and wrinkles, whereas the impermeability of graphene was exploited to seal larger defects using interfacial polymerization, where monomers introduced on opposite sides of the graphene layer react to form polymer plugs only where graphene is missing (Fig. 5b). After introducing subnanometre pores by ion irradiation and etching, the resulting membrane exhibited water permeance based on graphene area comparable to polyamide reverse osmosis membranes, and rejected organic molecules (≥1 nm) and divalent $MgSO_4$ (but not NaCl) under osmotically driven flow (Fig. 5d).

Beyond these considerations, an appropriate support layer is essential to achieve high selectivity in the presence of imperfections and defects[173]. An ideal support — or coating — will add a transport resistance in series to both selective pores and defects, thereby limiting leakage without adversely impacting the permeance. This resistive layer must provide parallel transport pathways or be thinner than the spacing between non-selective defects in the atomically thin layer[173]. Such an approach was critical to early commercialization of gas separation membranes[11]. Beyond its role in minimizing leakage, the support must have high surface porosity to make use of most of the NATM area, have high mechanical strength, good chemical resistance, higher permeance than the atomically thin layer, and provide stable adhesion and facilitate transfer or coating of the atomically thin layer. Most experimental studies have used specialized supports (for example, polycarbonate track-etched membranes[123] or microfabricated silicon supports[46]) with low surface porosity, which results in high permeance with respect to graphene area but low permeance based on total membrane area, and are suboptimal for practical separations. Although graphene NATMs have been fabricated on more practical supports such as poly(1-methylsilyl-1-propyne)[179], polypropylene[180] and polyvinylidenedifluoride[180], meeting all of the above requirements is challenging, especially for pressure-driven separations.

Potential applications of NATMs

The path for new membrane technologies to advance beyond the laboratory is tortuous[1]. Membranes that are difficult to scale up have found use in research and analytical applications[181], whereas polyamide reverse osmosis membranes have grown to become the dominant desalination technology today. Although NATMs are still in the early stages of development, they present characteristics that are potentially advantageous for addressing persistent challenges in membrane separations.

A key advantage of NATMs is their high permeance that could enable higher energy efficiency and compact, high-productivity membrane separation systems. For seawater and brackish water, respectively, increasing the permeance of desalination membranes threefold could reduce the membrane area by 44% and 63% or reduce the energy consumption by 15% and 46% (ref. 182); the smaller gains for seawater are due to its higher osmotic pressure and build-up of the rejected salt at the membrane. More substantial gains in energy consumption and productivity are expected for applications involving low solute concentrations (for example, reverse osmosis treatment for drinking water, ultrapure water, and nanofiltration for water, pharmaceutical, food and beverage, and biotechnology industries[13,183]), provided that fouling is not enhanced at higher fluxes[184]. The combination of high selectivity and permeance is also desirable for a number of gas separations[19], such as O_2 or N_2 from air, CO_2/CH_4 for natural gas sweetening and H_2O/air for dehumidification[185].

A second advantage of NATMs is their potential for increased robustness due to high chemical resistance and mechanical strength, which could prove useful for operation under harsh conditions. For example, NATMs may be able to better withstand chlorine and permit desalination of high-salinity water by high-pressure reverse osmosis, or allow for more aggressive cleaning procedures[184] to maintain membrane performance and extend their useful life. NATMs may help to address the challenges of aging, compaction and influence of solvents in organic solvent nanofiltration[13], and potentially open new possibilities in the separation of liquefied gases and fuels.

Third, the molecular-sieving mechanism of transport is expected to lead to rejection of all species that significantly exceed the pore size[99,101]. If NATMs could provide universal size-based rejection regardless of the solute or the fluid in which separation is performed, it would benefit applications involving a diversity of solutes such as in removal of persistent organic pollutants[8,10] for water reclamation, removal of boron from seawater[17] or in chemical processing[3,13].

However, actual application is contingent on commensurate advances in technology and practical membranes meeting these expectations[41]. The predicted performance and most of the proposed applications have yet to be realized even at the lab scale. Significant advances including ensuring a tight pore size distribution, design of appropriate supports and minimizing leakage are prerequisite for proof-of-concept studies. Manufacture at appropriate scale and cost, packaging into modules that minimize concentration polarization[186], characterization of fouling and chemical resistance, and demonstration of long-term performance under realistic conditions are essential[41] for large-scale applications such as water desalination and natural gas separations. Small-scale applications such as laboratory and analytical separations or nanofiltration — which have less stringent demands on selectivity but would benefit from the high permeance and chemical stability of NATMs — are likely to emerge first.

Beyond separations, NATMs could find use in a variety of other applications such as in fuel cells[130,132,133], microfluidics[111], sensing[16], surface micropatterning[187], energy harvesting[129] and a variety of biomedical applications, such as drug release, biosensing and immunoisolation[12]. Nanopores in NATMs may find use in detection and analysis of single molecules, ions and binding events, or interrogating discrete steps in chemical reactions[165]. In these applications, NATMs have the potential to offer higher selectivity, sensitivity, faster time-to-result or ease of fabrication. The more exotic capabilities of NATMs, such as isotope separation by quantum effects[131] and perhaps undiscovered phenomena that do not have parallels in other membranes, could potentially open new applications. Finally, NATMs can provide fundamental insights into nanofluidic transport mechanisms that are relevant to atomically thin materials for barrier applications[188], for electron microscopy[189] and in graphene oxide membranes[32].

Future perspectives

Regardless of the extent and timeframe in which NATMs will have an impact, they represent a unique class of membrane with tremendous potential for advancing membrane technology and are likely to persist far into the future.

Although theoretical studies have shed light on transport mechanisms in idealized pores, an understanding of the structure and behaviour of pores in real materials has only just started to emerge. Controlled experiments at the single pore level, complemented by theoretical studies on realistic pores, are required to probe the effects of different pore structures, functional groups, dynamic behaviours and the role of surface contaminants. Simulations are needed to advance pore creation techniques and explore different applications of NATMs, which can guide experimental developments. For example, are there pore structures that enable selective transport of water over boron, urea and other species that are difficult to reject using state-of-the-art membranes? Can NATMs separate water from ethanol? How effective are NATMs for separations in organic solvents?

Realization of practical membranes requires advances on four fronts. First, improved methods are needed to create a high density of uniform pores that will enable separations such as water desalination. Here, key challenges are achieving sufficiently precise pores using top-down techniques and scale-up of bottom-up synthesis methods. Second, better understanding of the origin of defects that

may arise during synthesis, handling or creation of selective pores, methods to limit leakage through defects, and quality control during synthesis are indispensable for realization of functional membranes. Theoretical studies are needed that shed light on how the distribution of pore size and defects as well as the membrane support structure determine the actual permeance and selectivity. Third, design or selection of an appropriate porous support layer and development of methods to promote adhesion and to coat the atomically thin layer on the support are essential for full utilization of the properties of NATMs. Fourth, packaging of membranes, design of modules tailored to NATMs, experimental and theoretical studies to understand fouling, chemical resistance, and potential degradation mechanisms, and cost-effective scale-up of membrane manufacturing are critical for advancing NATMs towards real-world applications.

Finally, it is likely that there will be opportunities to use NATMs in novel formats or in novel devices. For example, NATMs could act as porous scaffolds to realize novel membranes with improved performance by coating[190] or functionalizing[191] them with ultrathin layers of materials[192], perhaps by grafting polymers or materials that are difficult to cast into thin membranes. The fact that it is possible to make NATMs from conducting as well as insulating atomically thin materials raises the possibility of electrically actuated membranes that can actively modulate transport or pump ions[9]. Other intriguing possibilities arise due to the atomically thin nature that enables reactions across pores in NATMs — which could find use in selectively sealing leaky pores, functionalizing the membranes or performing chemical reactions across NATMs where pores control the stereochemistry.

Although significant technological challenges remain for practical applications, NATMs have provided us with the fascinating opportunity to explore fundamental questions in fluid flow at the smallest possible length scale. It is quite likely that these fundamental studies will continue to provide new — and perhaps surprising — insights into mass transport at the nanoscale. On the practical side, NATMs have tremendous potential, but also face considerable challenges that need to be recognized and addressed if the field is to move ahead. Only time will reveal whether NATMs live up to their promise.

Received 8 March 2016; accepted 20 March 2017; published online 6 June 2017

References

1. Baker, R. W. & Low, B. T. Gas separation membrane materials: a perspective. *Macromolecules* **47,** 6999–7013 (2014).
2. Baker, R. W. *Membrane Technology and Applications* (John Wiley & Sons, 2004).
3. Buonomenna, M. G. Membrane processes for a sustainable industrial growth. *RSC Adv.* **3,** 5694–5740 (2013).
4. Wang, Y., Chen, K. S., Mishler, J., Cho, S. C. & Adroher, X. C. A review of polymer electrolyte membrane fuel cells: technology, applications, and needs on fundamental research. *Appl. Energy* **88,** 981–1007 (2011).
5. Geise, G. M. *et al.* Water purification by membranes: the role of polymer science. *J. Polym. Sci., Polym. Phys.* **48,** 1685–1718 (2010).
6. Mohammad, A. W., Ng, C. Y., Lim, Y. P. & Ng, G. H. Ultrafiltration in food processing industry: review on application, membrane fouling, and fouling control. *Food Bioprocess Technol.* **5,** 1143–1156 (2012).
7. van Reis, R. & Zydney, A. Bioprocess membrane technology. *J. Membrane Sci.* **297,** 16–50 (2007).
8. Greenlee, L. F., Lawler, D. F., Freeman, B. D., Marrot, B. & Moulin, P. Reverse osmosis desalination: water sources, technology, and today's challenges. *Water Res.* **43,** 2317–2348 (2009).
9. Shannon, M. A. *et al.* Science and technology for water purification in the coming decades. *Nature* **452,** 301–310 (2008).
10. Malaeb, L. & Ayoub, G. M. Reverse osmosis technology for water treatment: state of the art review. *Desalination* **267,** 1–8 (2011).
11. Baker, R. W. Future directions of membrane gas separation technology. *Ind. Eng. Chem. Res.* **41,** 1393–1411 (2002).
12. Stamatialis, D. F. *et al.* Medical applications of membranes: drug delivery, artificial organs and tissue engineering. *J. Membrane Sci.* **308,** 1–34 (2008).
13. Marchetti, P., Jimenez Solomon, M. F., Szekely, G. & Livingston, A. G. Molecular separation with organic solvent nanofiltration: a critical review. *Chem. Rev.* **114,** 10735–10806 (2014).
14. Takht Ravanchi, M., Kaghazchi, T. & Kargari, A. Application of membrane separation processes in petrochemical industry: a review. *Desalination* **235,** 199–244 (2009).
15. Pendergast, M. M. & Hoek, E. M. V. A review of water treatment membrane nanotechnologies. *Energy Environ. Sci.* **4,** 1946–1971 (2011).
16. De Marco, R., Clarke, G. & Pejcic, B. Ion-selective electrode potentiometry in environmental analysis. *Electroanalysis* **19,** 1987–2001 (2007).
17. Elimelech, M. & Phillip, W. A. The future of seawater desalination: energy, technology, and the environment. *Science* **333,** 712–717 (2011).
18. Tavolaro, A. & Drioli, E. Zeolite membranes. *Adv. Mater.* **11,** 975–996 (1999).
19. Buonomenna, M. G., Yave, W. & Golemme, G. Some approaches for high performance polymer based membranes for gas separation: block copolymers, carbon molecular sieves and mixed matrix membranes. *RSC Adv.* **2,** 10745–10773 (2012).
20. Furukawa, H., Cordova, K. E., O'Keeffe, M. & Yaghi, O. M. The chemistry and applications of metal-organic frameworks. *Science* **341,** 1230444 (2013).
21. Holt, J. K. *et al.* Fast mass transport through sub-2-nanometer carbon nanotubes. *Science* **312,** 1034–1037 (2006).
22. Anselmetti, D. & Gölzhäuser, A. Converting molecular monolayers into functional membranes. *Angew. Chem. Int. Ed.* **53,** 12300–12302 (2014).
23. Das, R., Ali, M. E., Hamid, S. B. A., Ramakrishna, S. & Chowdhury, Z. Z. Carbon nanotube membranes for water purification: a bright future in water desalination. *Desalination* **336,** 97–109 (2014).
24. Kim, S. & Lee, Y. M. Rigid and microporous polymers for gas separation membranes. *Prog. Polym. Sci.* **43,** 1–32 (2015).
25. Geim, A. K. & Novoselov, K. S. The rise of graphene. *Nat. Mater.* **6,** 183–191 (2007).
26. Bunch, J. S. *et al.* Impermeable atomic membranes from graphene sheets. *Nano Lett.* **8,** 2458–2462 (2008).
This study experimentally demonstrated the impermeability of pristine graphene.
27. Lee, C., Wei, X., Kysar, J. W. & Hone, J. Measurement of the elastic properties and intrinsic strength of monolayer graphene. *Science* **321,** 385–388 (2008).
28. Chen, Y., Zou, J., Campbell, S. J. & Le Caer, G. Boron nitride nanotubes: pronounced resistance to oxidation. *Appl. Phys. Lett.* **84,** 2430–2432 (2004).
29. Koenig, S. P., Wang, L., Pellegrino, J. & Bunch, J. S. Selective molecular sieving through porous graphene. *Nat. Nanotech.* **7,** 728–732 (2012).
This study experimentally realized molecular sieving across atomically thin membranes.
30. Zhao, Y. *et al.* Two-dimensional material membranes: an emerging platform for controllable mass transport applications. *Small* **10,** 4521–4542 (2014).
31. Aghigh, A. *et al.* Recent advances in utilization of graphene for filtration and desalination of water: a review. *Desalination* **365,** 389–397 (2015).
32. Yoon, H. W., Cho, Y. H. & Park, H. B. Graphene-based membranes: status and prospects. *Philos. Trans. R. Soc. A* **374,** 20150024 (2016).
33. Mahmoud, K. A., Mansoor, B., Mansour, A. & Khraisheh, M. Functional graphene nanosheets: the next generation membranes for water desalination. *Desalination* **356,** 208–225 (2015).
34. Sun, C., Wen, B. & Bai, B. Recent advances in nanoporous graphene membrane for gas separation and water purification. *Sci. Bull.* **60,** 1807–1823 (2015).
35. Huang, L., Zhang, M., Li, C. & Shi, G. Graphene-based membranes for molecular separation. *J. Phys. Chem. Lett.* **6,** 2806–2815 (2015).
36. Sun, P., Wang, K. & Zhu, H. Recent developments in graphene-based membranes: structure, mass-transport mechanism and potential applications. *Adv. Mater.* **28,** 2287–2310 (2016).
37. Cohen-Tanugi, D. & Grossman, J. C. Nanoporous graphene as a reverse osmosis membrane: recent insights from theory and simulation. *Desalination* **366,** 59–70 (2015).
38. Hegab, H. M. & Zou, L. Graphene oxide-assisted membranes: fabrication and potential applications in desalination and water purification. *J. Membrane Sci.* **484,** 95–106 (2015).
39. Liu, G., Jin, W. & Xu, N. Graphene-based membranes. *Chem. Soc. Rev.* **44,** 5016–5030 (2015).
40. Mi, B. Graphene oxide membranes for ionic and molecular sieving. *Science* **343,** 740–742 (2014).
41. Goh, P. S. & Ismail, A. F. Graphene-based nanomaterial: the state-of-the-art material for cutting edge desalination technology. *Desalination* **356,** 115–128 (2015).
42. Yampolskii, Y. Polymeric gas separation membranes. *Macromolecules* **45,** 3298–3311 (2012).
43. Robeson, L. M. The upper bound revisited. *J. Membrane Sci.* **320,** 390–400 (2008).
44. Freeman, B. D. Basis of permeability/selectivity tradeoff relations in polymeric gas separation membranes. *Macromolecules* **32,** 375–380 (1999).
45. Bernardo, P., Drioli, E. & Golemme, G. Membrane gas separation: a review/state of the art. *Ind. Eng. Chem. Res.* **48,** 4638–4663 (2009).

46. Celebi, K. *et al.* Ultimate permeation across atomically thin porous graphene. *Science* **344,** 289–292 (2014).
This study demonstrated fabrication of arrays of nanopores in graphene membranes using a focused ion beam to realize high permeance.
47. Szymczyk, A. & Fievet, P. Investigating transport properties of nanofiltration membranes by means of a steric, electric and dielectric exclusion model. *J. Membrane Sci.* **252,** 77–88 (2005).
48. Jiang, D., Cooper, V. R. & Dai, S. Porous graphene as the ultimate membrane for gas separation. *Nano Lett.* **9,** 4019–4024 (2009).
This simulation study suggested the potential of nanoporous graphene for gas separation with high selectivity and permeance.
49. Du, H. *et al.* Separation of hydrogen and nitrogen gases with porous graphene membrane. *J. Phys. Chem. C* **115,** 23261–23266 (2011).
50. Schrier, J. Helium separation using porous graphene membranes. *J. Phys. Chem. Lett.* **1,** 2284–2287 (2010).
51. Blankenburg, S. *et al.* Porous graphene as an atmospheric nanofilter. *Small* **6,** 2266–2271 (2010).
52. Huang, C., Wu, H., Deng, K., Tang, W. & Kan, E. Improved permeability and selectivity in porous graphene for hydrogen purification. *Phys. Chem. Chem. Phys.* **16,** 25755–25759 (2014).
53. Brockway, A. M. & Schrier, J. Noble gas separation using PG-ES X (X = 1, 2, 3) nanoporous two-dimensional polymers. *J. Phys. Chem. C* **117,** 393–402 (2013).
54. Solvik, K., Weaver, J. A., Brockway, A. M. & Schrier, J. Entropy-driven molecular separations in 2D-nanoporous materials, with application to high-performance paraffin/olefin membrane separations. *J. Phys. Chem. C* **117,** 17050–17057 (2013).
55. Tao, Y. *et al.* Tunable hydrogen separation in porous graphene membrane: first-principle and molecular dynamic simulation. *ACS Appl. Mater. Interfaces* **6,** 8048–8058 (2014).
56. Schrier, J. Carbon dioxide separation with a two-dimensional polymer membrane. *ACS Appl. Mater. Interfaces* **4,** 3745–3752 (2012).
57. Cranford, S. W. & Buehler, M. J. Selective hydrogen purification through graphdiyne under ambient temperature and pressure. *Nanoscale* **4,** 4587–4593 (2012).
58. Jiao, Y. *et al.* Graphdiyne: a versatile nanomaterial for electronics and hydrogen purification. *Chem. Commun.* **47,** 11843–11845 (2011).
59. Zhang, H. *et al.* Tunable hydrogen separation in sp–sp^2 hybridized carbon membranes: a first-principles prediction. *J. Phys. Chem. C* **116,** 16634–16638 (2012).
60. Schrier, J. Fluorinated and nanoporous graphene materials as sorbents for gas separations. *ACS Appl. Mater. Interfaces* **3,** 4451–4458 (2011).
61. Li, Y., Zhou, Z., Shen, P. & Chen, Z. Two-dimensional polyphenylene: experimentally available porous graphene as a hydrogen purification membrane. *Chem. Commun.* **46,** 3672–3674 (2010).
62. Schrier, J. & McClain, J. Thermally-driven isotope separation across nanoporous graphene. *Chem. Phys. Lett.* **521,** 118–124 (2012).
63. Tian, Z., Dai, S. & Jiang, D. Expanded porphyrins as two-dimensional porous membranes for CO_2 separation. *ACS Appl. Mater. Interfaces* **7,** 13073–13079 (2015).
64. Zhang, Y. *et al.* Hexagonal boron nitride with designed nanopores as a high-efficiency membrane for separating gaseous hydrogen from methane. *J. Phys. Chem. C* **119,** 19826–19831 (2015).
65. Liu, H., Dai, S. & Jiang, D. Permeance of H_2 through porous graphene from molecular dynamics. *Solid State Commun.* **175–176,** 101–105 (2013).
66. Jiao, Y., Du, A., Hankel, M. & Smith, S. C. Modelling carbon membranes for gas and isotope separation. *Phys. Chem. Chem. Phys.* **15,** 4832–4843 (2013).
67. Drahushuk, L. W. & Strano, M. S. Mechanisms of gas permeation through single layer graphene membranes. *Langmuir* **28,** 16671–16678 (2012).
68. Sun, C. *et al.* Mechanisms of molecular permeation through nanoporous graphene membranes. *Langmuir* **30,** 675–682 (2014).
69. Hauser, A. W. & Schwerdtfeger, P. Nanoporous graphene membranes for efficient ^{3}He/^{4}He separation. *J. Phys. Chem. Lett.* **3,** 209–213 (2012).
70. Hankel, M., Jiao, Y., Du, A., Gray, S. K. & Smith, S. C. Asymmetrically decorated, doped porous graphene as an effective membrane for hydrogen isotope separation. *J. Phys. Chem. C* **116,** 6672–6676 (2012).
71. Hu, W., Wu, X., Li, Z. & Yang, J. Porous silicene as a hydrogen purification membrane. *Phys. Chem. Chem. Phys.* **15,** 5753–5757 (2013).
72. Lalitha, M., Lakshmipathi, S. & Bhatia, S. K. Defect-mediated reduction in barrier for helium tunneling through functionalized graphene nanopores. *J. Phys. Chem. C* **119,** 20940–20948 (2015).
73. Au, H. *Molecular Dynamics Simulation of Nanoporous Graphene for Selective Gas Separation* (Massachusetts Institute of Technology, 2012).
74. Lei, G., Liu, C., Xie, H. & Song, F. Separation of the hydrogen sulfide and methane mixture by the porous graphene membrane: effect of the charges. *Chem. Phys. Lett.* **599,** 127–132 (2014).
75. Liu, H., Chen, Z., Dai, S. & Jiang, D. Selectivity trend of gas separation through nanoporous graphene. *J. Solid State Chem.* **224,** 2–6 (2015).
76. Liu, H., Dai, S. & Jiang, D. Insights into CO_2/N_2 separation through nanoporous graphene from molecular dynamics. *Nanoscale* **5,** 9984–9987 (2013).
77. Shan, M. *et al.* Influence of chemical functionalization on the CO_2/N_2 separation performance of porous graphene membranes. *Nanoscale* **4,** 5477–5482 (2012).
78. Sun, C., Wen, B. & Bai, B. Application of nanoporous graphene membranes in natural gas processing: molecular simulations of CH_4/CO_2, CH_4/H_2S and CH_4/N_2 separation. *Chem. Eng. Sci.* **138,** 616–621 (2015).
79. Wen, B., Sun, C. & Bai, B. Inhibition effect of a non-permeating component on gas permeability of nanoporous graphene membranes. *Phys. Chem. Chem. Phys.* **17,** 23619–23626 (2015).
80. Wu, T. *et al.* Fluorine-modified porous graphene as membrane for CO_2 /N_2 separation: molecular dynamic and first-principles simulations. *J. Phys. Chem. C* **118,** 7369–7376 (2014).
81. Qin, X., Meng, Q., Feng, Y. & Gao, Y. Graphene with line defect as a membrane for gas separation: design via a first-principles modeling. *Surf. Sci.* **607,** 153–158 (2013).
82. Hauser, A. W. & Schwerdtfeger, P. Methane-selective nanoporous graphene membranes for gas purification. *Phys. Chem. Chem. Phys.* **14,** 13292–13298 (2012).
83. Ambrosetti, A. & Silvestrelli, P. L. Gas separation in nanoporous graphene from first principle calculations. *J. Phys. Chem. C* **118,** 19172–19179 (2014).
84. Lu, R. *et al.* Prominently improved hydrogen purification and dispersive metal binding for hydrogen storage by substitutional doping in porous graphene. *J. Phys. Chem. C* **116,** 21291–21296 (2012).
85. Hauser, A. W., Schrier, J. & Schwerdtfeger, P. Helium tunneling through nitrogen-functionalized graphene pores: pressure- and temperature-driven approaches to isotope separation. *J. Phys. Chem. C* **116,** 10819–10827 (2012).
86. Wang, L. *et al.* Molecular valves for controlling gas phase transport made from discrete ångström-sized pores in graphene. *Nat. Nanotech.* **10,** 785–790 (2015).
87. Drahushuk, L. W., Wang, L., Koenig, S. P., Bunch, J. S. & Strano, M. S. Analysis of time-varying, stochastic gas transport through graphene membranes. *ACS Nano* **10,** 786–795 (2016).
88. Jain, T. *et al.* Heterogeneous sub-continuum ionic transport in statistically isolated graphene nanopores. *Nat. Nanotech.* **10,** 1053–1057 (2015).
89. Zhu, C., Li, H., Zeng, X. C., Wang, E. G. & Meng, S. Quantized water transport: ideal desalination through graphyne-4 membrane. *Sci. Rep.* **3,** 3163 (2013).
90. Xue, M., Qiu, H. & Guo, W. Exceptionally fast water desalination at complete salt rejection by pristine graphyne monolayers. *Nanotechnology* **24,** 505720 (2013).
91. Bartolomei, M. *et al.* Penetration barrier of water through graphynes' pores: first-principles predictions and force field optimization. *J. Phys. Chem. Lett.* **5,** 751–755 (2014).
92. Kou, J., Zhou, X., Lu, H., Wu, F. & Fan, J. Graphyne as the membrane for water desalination. *Nanoscale* **6,** 1865–1870 (2014).
93. Heiranian, M., Farimani, A. B. & Aluru, N. R. Water desalination with a single-layer MoS_2 nanopore. *Nat. Commun.* **6,** 8616 (2015).
94. Lin, L.-C., Choi, J. & Grossman, J. C. Two-dimensional covalent triazine framework as an ultrathin-film nanoporous membrane for desalination. *Chem. Commun.* **51,** 14921–14924 (2015).
95. Konatham, D., Yu, J., Ho, T. A. & Striolo, A. Simulation insights for graphene-based water desalination membranes. *Langmuir* **29,** 11884–11897 (2013).
96. Cohen-Tanugi, D. & Grossman, J. C. Water desalination across nanoporous graphene. *Nano Lett.* **12,** 3602–3608 (2012).
This molecular dynamics study showed the potential of graphene for water desalination with high salt rejection and high permeance.
97. Li, W., Yang, Y., Weber, J. K., Zhang, G. & Zhou, R. Tunable, strain-controlled nanoporous MoS_2 filter for water desalination. *ACS Nano* **10,** 1829–1835 (2016).
98. Cohen-Tanugi, D. & Grossman, J. C. Water permeability of nanoporous graphene at realistic pressures for reverse osmosis desalination. *J. Chem. Phys.* **141,** 074704 (2014).
99. Azamat, J., Khataee, A. & Joo, S. W. Molecular dynamics simulation of trihalomethanes separation from water by functionalized nanoporous graphene under induced pressure. *Chem. Eng. Sci.* **127,** 285–292 (2015).
100. Suk, M. E. & Aluru, N. R. Water transport through ultrathin graphene. *J. Phys. Chem. Lett.* **1,** 1590–1594 (2010).
101. Lin, S. & Buehler, M. J. Mechanics and molecular filtration performance of graphyne nanoweb membranes for selective water purification. *Nanoscale* **5,** 11801–11807 (2013).
102. Suk, M. E. & Aluru, N. R. Molecular and continuum hydrodynamics in graphene nanopores. *RSC Adv.* **3,** 9365–9372 (2013).
103. Song, Z. & Xu, Z. Ultimate osmosis engineered by the pore geometry and functionalization of carbon nanostructures. *Sci. Rep.* **5,** 10597 (2015).
104. Zhang, X. & Gai, J.-G. Single-layer graphyne membranes for super-excellent brine separation in forward osmosis. *RSC Adv.* **5,** 68109–68116 (2015).
105. Gai, J.-G., Gong, X.-L., Wang, W.-W., Zhang, X. & Kang, W.-L. An ultrafast water transport forward osmosis membrane: porous graphene. *J. Mater. Chem. A* **2,** 4023–4028 (2014).

106. Gai, J. & Gong, X. Zero internal concentration polarization FO membrane: functionalized graphene. *J. Mater. Chem. A* **2,** 425–429 (2014).
107. He, Z., Zhou, J., Lu, X. & Corry, B. Bioinspired graphene nanopores with voltage-tunable ion selectivity for Na^+ and K^+. *ACS Nano* **7,** 10148–10157 (2013).
108. Kang, Y. *et al.* Na^+ and K^+ ion selectivity by size-controlled biomimetic graphene nanopores. *Nanoscale* **6,** 10666–10672 (2014).
109. Sint, K., Wang, B. & Král, P. Selective ion passage through functionalized graphene nanopores. *J. Am. Chem. Soc.* **131,** 9600–9600 (2009).
110. Suk, M. E. & Aluru, N. R. Ion transport in sub-5-nm graphene nanopores. *J. Chem. Phys.* **140,** 084707 (2014).
111. Zhao, S., Xue, J. & Kang, W. Ion selection of charge-modified large nanopores in a graphene sheet. *J. Chem. Phys.* **139,** 114702 (2013).
112. Zhu, C., Li, H. & Meng, S. Transport behavior of water molecules through two-dimensional nanopores. *J. Chem. Phys.* **141,** 18C528 (2014).
113. Kou, J. *et al.* Water permeation through single-layer graphyne membrane. *J. Chem. Phys.* **139,** 064705 (2013).
114. Chandra Shekar, S. & Swathi, R. S. Rattling motion of alkali metal ions through the cavities of model compounds of graphyne and graphdiyne. *J. Phys. Chem. A* **117,** 8632–8641 (2013).
115. Garnier, L., Szymczyk, A., Malfreyt, P., & Ghoufi, A. Physics behind water transport through nanoporous boron nitride and graphene. *J. Phys. Chem. Lett.* **7,** 3371–3376 (2016).
116. Park, H. G. & Jung, Y. Carbon nanofluidics of rapid water transport for energy applications. *Chem. Soc. Rev.* **43,** 565–76 (2014).
117. Garaj, S. *et al.* Graphene as a subnanometre trans-electrode membrane. *Nature* **467,** 190–193 (2010).
This paper reported ionic transport and DNA sensing across graphene nanopores, and experimentally showed hydration energy-dependent ion transport across graphene.
118. Schneider, G. F. *et al.* DNA translocation through graphene nanopores. *Nano Lett.* **10,** 3163–3167 (2010).
119. Merchant, C. A. *et al.* DNA translocation through graphene nanopores. *Nano Lett.* **10,** 2915–2921 (2010).
120. O'Hern, S. C. *et al.* Selective molecular transport through intrinsic defects in a single layer of CVD graphene. *ACS Nano* **6,** 10130–10138 (2012).
121. O'Hern, S. C. *et al.* Selective ionic transport through tunable subnanometer pores in single-layer graphene membranes. *Nano Lett.* **14,** 1234–1241 (2014).
122. Surwade, S. P. *et al.* Water desalination using nanoporous single-layer graphene. *Nat. Nanotech.* **10,** 459–64 (2015).
This paper demonstrated facile pore creation in graphene using oxygen plasma to realize water desalination membranes.
123. O'Hern, S. C. *et al.* Nanofiltration across defect-sealed nanoporous monolayer graphene. *Nano Lett.* **15,** 3254–3260 (2015).
This paper reported nanofiltration across graphene enabled by defect sealing and creation of a high density of sub-nanometer pores.
124. Rollings, R. C., Kuan, A. T. & Golovchenko, J. A. Ion selectivity of graphene nanopores. *Nat. Commun.* **7,** 11408 (2016).
125. Liu, S. *et al.* Boron nitride nanopores: highly sensitive DNA single-molecule detectors. *Adv. Mater.* **25,** 4549–4554 (2013).
126. Liu, K., Feng, J., Kis, A. & Radenovic, A. Atomically thin molybdenum disulfide nanopores with high sensitivity for DNA translocation. *ACS Nano* **8,** 2504–2511 (2014).
127. Kuan, A. T., Lu, B., Xie, P., Szalay, T. & Golovchenko, J. A. Electrical pulse fabrication of graphene nanopores in electrolyte solution. *Appl. Phys. Lett.* **106,** 203109 (2015).
128. Feng, J. *et al.* Observation of ionic Coulomb blockade in nanopores. *Nat. Mater.* **15,** 850–855 (2016).
129. Feng, J. *et al.* Single-layer MoS_2 nanopores as nanopower generators. *Nature* **536,** 197–200 (2016).
130. Hu, S. *et al.* Proton transport through one-atom-thick crystals. *Nature* **516,** 227–230 (2014).
131. Lozada-Hidalgo, M. *et al.* Sieving hydrogen isotopes through two-dimensional crystals. *Science* **351,** 68–70 (2016).
This study experimentally demonstrated hydrogen isotope separation across atomically thin membranes.
132. Walker, M. I., Braeuninger-Weimer, P., Weatherup, R. S., Hofmann, S. & Keyser, U. F. Measuring the proton selectivity of graphene membranes. *Appl. Phys. Lett.* **107,** 213104 (2015).
133. Achtyl, J. L. *et al.* Aqueous proton transfer across single-layer graphene. *Nat. Commun.* **6,** 6539 (2015).
134. Ferrari, A. C. *et al.* Science and technology roadmap for graphene, related two-dimensional crystals, and hybrid systems. *Nanoscale* **7,** 4598–4810 (2014).
135. Li, X. S. *et al.* Large-area synthesis of high-quality and uniform graphene films on copper foils. *Science* **324,** 1312–1314 (2009).
136. Bae, S. *et al.* Roll-to-roll production of 30-inch graphene films for transparent electrodes. *Nat. Nanotech.* **5,** 574–578 (2010).
137. Kobayashi, T. *et al.* Production of a 100-m-long high-quality graphene transparent conductive film by roll-to-roll chemical vapor deposition and transfer process. *Appl. Phys. Lett.* **102,** 23112 (2013).
This paper reported the synthesis of graphene and its transfer to a polymeric support in a scalable roll-to-roll process.
138. Zaretski, A. V & Lipomi, D. J. Processes for non-destructive transfer of graphene: widening the bottleneck for industrial scale production. *Nanoscale* **7,** 9963–9969 (2015).
139. Waduge, P. *et al.* Direct and scalable deposition of atomically thin low-noise MoS_2 membranes on apertures. *ACS Nano* **9,** 7352–7359 (2015).
140. Alemán, B. *et al.* Transfer-free batch fabrication of large-area suspended graphene membranes. *ACS Nano* **4,** 4762–4768 (2010).
141. Lehtinen, O. *et al.* Production of defects in hexagonal boron nitride monolayer under ion irradiation. *Nucl. Instrum. Methods B* **269,** 1327–1331 (2011).
142. Lehtinen, O., Kotakoski, J., Krasheninnikov, A. V. & Keinonen, J. Cutting and controlled modification of graphene with ion beams. *Nanotechnology* **22,** 175306 (2011).
143. Lehtinen, O. *et al.* Non-invasive transmission electron microscopy of vacancy defects in graphene produced by ion irradiation. *Nanoscale* **6,** 6569–6576 (2014).
144. Lucchese, M. M. *et al.* Quantifying ion-induced defects and Raman relaxation length in graphene. *Carbon* **48,** 1592–1597 (2010).
145. Russo, C. J. & Golovchenko, J. A. Atom-by-atom nucleation and growth of graphene nanopores. *Proc. Natl Acad. Sci. USA* **109,** 5953–5957 (2012).
146. Tracz, A., Kalachev, A., Wegner, G. & Rabe, J. P. Control over nanopits on the basal plane of graphite by remote argon plasma and subsequent thermal oxidation. *Langmuir* **11,** 2840–2842 (1995).
147. Zabihi, Z. & Araghi, H. Formation of nanopore in a suspended graphene sheet with argon cluster bombardment: a molecular dynamics simulation study. *Nucl. Instrum. Methods B* **343,** 48–51 (2015).
148. Rozada, R. *et al.* Controlled generation of atomic vacancies in chemical vapor deposited graphene by microwave oxygen plasma. *Carbon* **79,** 664–669 (2014).
149. Xie, G. *et al.* A general route towards defect and pore engineering in graphene. *Small* **10,** 2280–2284 (2014).
150. Yamada, Y. *et al.* Subnanometer vacancy defects introduced on graphene by oxygen gas. *J. Am. Chem. Soc.* **136,** 2232–2235 (2014).
151. Zandiatashbar, A. *et al.* Effect of defects on the intrinsic strength and stiffness of graphene. *Nat. Commun.* **5,** 3186 (2014).
152. Fan, Z. *et al.* Easy synthesis of porous graphene nanosheets and their use in supercapacitors. *Carbon* **50,** 1699–1703 (2012).
153. Bagri, A., Grantab, R., Medhekar, N. V & Shenoy, V. B. Stability and formation mechanisms of carbonyl-and hydroxyl-decorated holes in graphene oxide. *J. Phys. Chem. C* **114,** 12053–12061 (2010).
154. Tracz, A., Wegner, G. & Rabe, J. P. Scanning tunneling microscopy study of graphite oxidation in ozone-air mixtures. *Langmuir* **19,** 6807–6812 (2003).
155. Liu, L. *et al.* Graphene oxidation: thickness-dependent etching and strong chemical doping. *Nano Lett.* **8,** 1965–1970 (2008).
156. Tao, H., Moser, J., Alzina, F., Wang, Q. & Sotomayor-Torres, C. M. The morphology of graphene sheets treated in an ozone generator. *J. Phys. Chem. C* **115,** 18257–18260 (2011).
157. Lehtinen, O. *et al.* Effects of ion bombardment on a two-dimensional target: atomistic simulations of graphene irradiation. *Phys. Rev. B* **81,** 153401 (2010).
158. Feng, J. *et al.* Identification of single nucleotides in MoS_2 nanopores. *Nat. Nanotech.* **10,** 1070–1076 (2015).
159. He, K. *et al.* Controlled formation of closed-edge nanopores in graphene. *Nanoscale* **7,** 11602–11610 (2015).
160. Bai, J., Zhong, X., Jiang, S., Huang, Y. & Duan, X. Graphene nanomesh. *Nat. Nanotech.* **5,** 190–194 (2010).
161. Cun, H., Iannuzzi, M., Hemmi, A., Osterwalder, J. & Greber, T. Two-nanometer voids in single-layer hexagonal boron nitride: formation via the 'can-opener' effect and annihilation by self-healing. *ACS Nano* **8,** 7423–7431 (2014).
162. Lin, L.-C. & Grossman, J. C. Atomistic understandings of reduced graphene oxide as an ultrathin-film nanoporous membrane for separations. *Nat. Commun.* **6,** 8335 (2015).
163. Wang, W. L. *et al.* Direct observation of a long-lived single-atom catalyst chiseling atomic structures in graphene. *Nano Lett.* **14,** 450–455 (2014).
164. Zhou, D., Cui, Y., Xiao, P.-W., Jiang, M.-Y. & Han, B.-H. A general and scalable synthesis approach to porous graphene. *Nat. Commun.* **5,** 4716 (2014).
165. Feng, J. *et al.* Electrochemical reaction in single layer MoS_2: nanopores opened atom by atom. *Nano Lett.* **15,** 3431–3438 (2015).
166. Liu, X.-H., Guan, C.-Z., Wang, D. & Wan, L.-J. Graphene-like single-layered covalent organic frameworks: synthesis strategies and application prospects. *Adv. Mater.* **26,** 6912–6920 (2014).
167. Cai, S.-L. *et al.* The organic flatland-recent advances in synthetic 2D organic layers. *Adv. Mater.* **27,** 5762–5770 (2015).
168. Peng, Q. *et al.* New materials graphyne, graphdiyne, graphone, and graphane: review of properties, synthesis, and application in nanotechnology. *Nanotechnol. Sci. Appl.* **7,** 1–29 (2014).

169. Li, G. *et al.* Architecture of graphdiyne nanoscale films. *Chem. Commun.* **46,** 3256–3258 (2010).
170. Murray, D. J. *et al.* Large area synthesis of a nanoporous two-dimensional polymer at the air/water interface. *J. Am. Chem. Soc.* **137,** 3450–3453 (2015).
171. Kidambi, P. R. *et al.* The parameter space of graphene chemical vapor deposition on polycrystalline Cu. *J. Phys. Chem. C* **116,** 22492–22501 (2012).
172. Wei, D. C. *et al.* Synthesis of N-doped graphene by chemical vapor deposition and its electrical properties. *Nano Lett.* **9,** 1752–1758 (2009).
173. Boutilier, M. S. H. *et al.* Implications of permeation through intrinsic defects in graphene on the design of defect-tolerant membranes for gas separation. *ACS Nano* **8,** 841–849 (2014).
174. Liu, Y. & Chen, X. Mechanical properties of nanoporous graphene membrane. *J. Appl. Phys.* **115,** 034303 (2014).
175. Cohen-Tanugi, D. & Grossman, J. C. Mechanical strength of nanoporous graphene as a desalination membrane. *Nano Lett.* **14,** 6171–6178 (2014).
176. Bertolazzi, S., Brivio, J. & Kis, A. Stretching and breaking of ultrathin MoS_2. *ACS Nano* **5,** 9703–9709 (2011).
177. Koenig, S. P., Boddeti, N. G., Dunn, M. L. & Bunch, J. S. Ultrastrong adhesion of graphene membranes. *Nat. Nanotech.* **6,** 543–546 (2011).
178. Won, M.-S., Penkov, O. V. & Kim, D.-E. Durability and degradation mechanism of graphene coatings deposited on Cu substrates under dry contact sliding. *Carbon* **54,** 472–481 (2013).
179. Kim, H. W. *et al.* Selective gas transport through few-layered graphene and graphene oxide membranes. *Science* **342,** 91–95 (2013).
180. Kafiah, F. M. *et al.* Monolayer graphene transfer onto polypropylene and polyvinylidenedifluoride microfiltration membranes for water desalination. *Desalination* **388,** 29–37 (2016).
181. Ingham, C. J., ter Maat, J. & de Vos, W. M. Where bio meets nano: the many uses for nanoporous aluminum oxide in biotechnology. *Biotechnol. Adv.* **30,** 1089–1099 (2012).
182. Cohen-Tanugi, D., McGovern, R. K., Dave, S. H., Lienhard, J. H. & Grossman, J. C. Quantifying the potential of ultra-permeable membranes for water desalination. *Energy Environ. Sci.* **7,** 1134–1141 (2014).
183. Mohammad, A. W. *et al.* Nanofiltration membranes review: recent advances and future prospects. *Desalination* **356,** 226–254 (2015).
184. Zhao, D. & Yu, S. A review of recent advance in fouling mitigation of NF/RO membranes in water treatment: pretreatment, membrane modification, and chemical cleaning. *Desalin. Water Treat.* **5,** 870–891 (2015).
185. Darvishi, M. & Foroutan, M. Mechanism of water separation from a gaseous mixture via nanoporous graphene using molecular dynamics simulation. *RSC Adv.* **5,** 81282–81294 (2015).
186. Zamani, F., Chew, J. W., Akhondi, E., Krantz, W. B. & Fane, A. G. Unsteady-state shear strategies to enhance mass-transfer for the implementation of ultrapermeable membranes in reverse osmosis: a review. *Desalination* **356,** 328–348 (2015).
187. Gethers, M. L. *et al.* Holey graphene as a weed barrier for molecules. *ACS Nano* **9,** 10909–10915 (2015).
188. Böhm, S. Graphene against corrosion. *Nat. Nanotech.* **9,** 741–742 (2014).
189. Zurutuza, A. & Marinelli, C. Challenges and opportunities in graphene commercialization. *Nat. Nanotech.* **9,** 730–734 (2014).
190. Lee, J. & Aluru, N. R. Water-solubility-driven separation of gases using graphene membrane. *J. Membrane Sci.* **428,** 546–553 (2013).
191. Georgakilas, V. *et al.* Functionalization of graphene: covalent and non-covalent approaches, derivatives and applications. *Chem. Rev.* **112,** 6156–6214 (2012).
192. Wang, L. *et al.* Ultrathin oxide films by atomic layer deposition on graphene. *Nano Lett.* **12,** 3706–3710 (2012).
193. Luo, Y., Harder, E., Faibish, R. S. & Roux, B. Computer simulations of water flux and salt permeability of the reverse osmosis FT-30 aromatic polyamide membrane. *J. Membrane Sci.* **384,** 1–9 (2011).
194. Kowalczyk, P., Gauden, P. A., Terzyk, A. P. & Furmaniak, S. Microscopic model of carbonaceous nanoporous molecular sieves — anomalous transport in molecularly confined spaces. *Phys. Chem. Chem. Phys.* **12,** 11351–11361 (2010).
195. Kim, M., Ha, Y.-C., Nguyen, T. N., Choi, H. Y. & Kim, D. Extended self-ordering regime in hard anodization and its application to make asymmetric AAO membranes for large pitch-distance nanostructures. *Nanotechnology* **24,** 505304 (2013).
196. Li, J.-R., Kuppler, R. J. & Zhou, H.-C. Selective gas adsorption and separation in metal–organic frameworks. *Chem. Soc. Rev.* **38,** 1477–1504 (2009).
197. Angelova, P. *et al.* A universal scheme to convert aromatic molecular monolayers into functional carbon nanomembranes. *ACS Nano* **7,** 6489–6497 (2013).
198. Wang, E. N. & Karnik, R. Water desalination: graphene cleans up water. *Nat. Nanotech.* **7,** 552–554 (2012).
199. Suk, M. E., Raghunathan, A. V. & Aluru, N. R. Fast reverse osmosis using boron nitride and carbon nanotubes. *Appl. Phys. Lett.* **92,** 133120 (2008).
200. Zhu, F., Tajkhorshid, E. & Schulten, K. Pressure-induced water transport in membrane channels studied by molecular dynamics. *Biophys. J.* **83,** 154–160 (2002).
201. Zhu, F., Tajkhorshid, E. & Schulten, K. Theory and simulation of water permeation in aquaporin-1. *Biophys. J.* **86,** 50–57 (2004).
202. Wells, D. B., Belkin, M., Comer, J. & Aksimentiev, A. Assessing graphene nanopores for sequencing DNA. *Nano Lett.* **12,** 4117–4123 (2012).
203. Sathe, C., Zou, X., Leburton, J.-P. & Schulten, K. Computational investigation of DNA detection using graphene nanopores. *ACS Nano* **5,** 8842–8851 (2011).
204. Garaj, S., Liu, S., Golovchenko, J. A. & Branton, D. Molecule-hugging graphene nanopores. *Proc. Natl Acad. Sci. USA* **110,** 12192–12196 (2013).
205. *Reverse Osmosis (RO) Membrane* (SterliTech Corporation, 2016); https://www.sterlitech.com/reverse-osmosis-ro-membrane.html
206. Xu, P. *et al.* Rejection of emerging organic micropollutants in nanofiltration–reverse osmosis membrane applications. *Water Environ. Res.* **77,** 40–48 (2005).
207. Comerton, A. M., Andrews, R. C., Bagley, D. M. & Yang, P. Membrane adsorption of endocrine disrupting compounds and pharmaceutically active compounds. *J. Memb. Sci.* **303,** 267–277 (2007).
208. van der Bruggen, B. & Vandecasteele, C. Flux decline during nanofiltration of organic components in aqueous solution. *Environ. Sci. Technol.* **35,** 3535–3540 (2001).
209. Ahmad, A. L., Tan, L. S. & Shukor, S. R. A. Dimethoate and atrazine retention from aqueous solution by nanofiltration membranes. *J. Hazard. Mater.* **151,** 71–77 (2008).
210. *Ultrafiltration (UF) Membranes* (SterliTech Corporation, 2016); https://www.sterlitech.com/ultrafiltration-uf-membrane.html
211. Celik, E., Park, H., Choi, H. H. & Choi, H. H. Carbon nanotube blended polyethersulfone membranes for fouling control in water treatment. *Water Res.* **45,** 274–282 (2011).
212. de Vos, R. M. High-selectivity, high-flux silica membranes for gas separation. *Science* **279,** 1710–1711 (1998).
213. Elyassi, B., Sahimi, M. & Tsotsis, T. T. Silicon carbide membranes for gas separation applications. *J. Membr. Sci.* **288,** 290–297 (2007).
214. Guo, H., Zhu, G., Hewitt, I. J. & Qiu, S. 'Twin copper source' growth of metal–organic framework membrane: Cu3(BTC)2 with high permeability and selectivity for recycling H2. *J. Am. Chem. Soc.* **131,** 1646–1647 (2009).
215. Rezac, M. E. & Schöberl, B. Transport and thermal properties of poly(ether imide)/acetylene-terminated monomer blends. *J. Memb. Sci.* **156,** 211–222 (1999).
216. Tang, Z., Dong, J. & Nenoff, T. M. Internal surface modification of MFI-type zeolite membranes for high selectivity and high flux for hydrogen. *Langmuir* **25,** 4848–4852 (2009).
217. Li, P. *et al.* Recent developments in membranes for efficient hydrogen purification. *J. Membr. Sci.* **495,** 130–168 (2015).
218. Yilmaz, G. & Keskin, S. Predicting the performance of zeolite imidazolate framework/polymer mixed matrix membranes for CO2, CH4, and H2 separations using molecular simulations. *Ind. Eng. Chem. Res.* **51,** 14218–14228 (2012).
219. Kang, Z. *et al.* Highly selective sieving of small gas molecules by using an ultra-microporous metal–organic framework membrane. *Energy Environ. Sci.* **7,** 4053–4060 (2014).
220. Kim, S., Jinschek, J. R., Chen, H., Sholl, D. S. & Marand, E. Scalable fabrication of carbon nanotube/polymer nanocomposite membranes for high flux gas transport. *Nano Lett.* **7,** 2806–2811 (2007).
221. Kim, S., Pechar, T. W. & Marand, E. Poly(imide siloxane) and carbon nanotube mixed matrix membranes for gas separation. *Desalination* **192,** 330–339 (2006).
222. Yu, M., Funke, H. H., Falconer, J. L. & Noble, R. D. High density, vertically-aligned carbon nanotube membranes. *Nano Lett.* **9,** 225–229 (2009).
223. Li, Y., Liang, F., Bux, H., Yang, W. & Caro, J. Zeolitic imidazolate framework ZIF-7 based molecular sieve membrane for hydrogen separation. *J. Memb. Sci.* **354,** 48–54 (2010).

Acknowledgements

The authors acknowledge research collaborations and helpful discussions with S. C. O'Hern, T. Jain, T. Laoui, J.-C. Idrobo and J. Kong.

Additional information

Supplementary information is available in the online version of the paper. Reprints and permissions information is available online at www.nature.com/reprints. Publisher's note: Springer Nature remains neutral with regard to jurisdictional claims in published maps and institutional affiliations. Correspondence should be addressed to R.K.

Competing financial interests

R.K. is a co-founder and has equity in a start-up company aimed at commercializing graphene membranes.